

Master Thesis

**Exploring the existence of prebiotic species:  
ALMA observations of amine-containing  
organic molecule in star-forming regions.**

**Harumi Minamoto**

17M01629

Nomura Laboratory

Department of Earth and Planetary Sciences, Tokyo Institute of Technology

**January 21, 2019**



# Abstract

A variety of complex organic molecules have been observed for decades in the interstellar medium. Some of them are considered to be delivered to the primordial Earth by comets, and contributed to the chemical evolution leading to terrestrial life. One example of such prebiotic species is amino acid. Glycine, the simplest amino acid, has been detected in comet 67P/C-G but its presence in molecular clouds is still uncertain.

In this work we analyze the ALMA archival data toward 3 star-forming regions, Orion Kleinmann-Low nebula (hereafter Orion-KL), IRAS 16293-2422 (IRAS 16293), and L483, to search methylamine ( $\text{CH}_3\text{NH}_2$ ), which is suggested as precursors to glycine.

As a result of analysis, we found 8 candidate emission at the hot core region in Orion-KL. By using the rotation diagram method, we evaluated its tentative column density and rotational temperature to be  $5.5 \times 10^{14} \text{ cm}^{-2}$  and 93.3 K, respectively. On the other hand,  $\text{CH}_3\text{NH}_2$  is not detected and stringent upper limit column densities are determined in IRAS 16293 and L483.

# Contents

<b>Abstract</b>	<b>i</b>
<b>1 Introduction</b>	<b>1</b>
1.1 Glycine and methylamine . . . . .	1
1.2 Star forming region . . . . .	2
1.2.1 Orion Kleinmann-Low nebula . . . . .	2
1.2.2 IRAS 16293-2422 . . . . .	2
1.2.3 L483 . . . . .	2
1.3 Radio observation . . . . .	2
1.3.1 Atacama Large Millimeter Array . . . . .	3
1.4 Purpose of this work . . . . .	3
<b>2 Methylamine survey in Orion-KL</b>	<b>4</b>
2.1 Observation data . . . . .	4
2.2 Analysis . . . . .	5
2.2.1 Continuum Subtraction of SV data . . . . .	5
2.2.2 Line identification . . . . .	8
2.3 Results . . . . .	8
2.3.1 Transitions . . . . .	8
2.3.2 Distribution . . . . .	9
2.3.3 Spectrum . . . . .	17
2.4 Disucssion . . . . .	18

2.4.1	Column density and Rotation temperature . . . . .	18
2.4.2	Blending . . . . .	19
<b>3</b>	<b>Methylamine survey in low mass star-forming regions</b>	<b>21</b>
3.1	Review of low mass star-forming region . . . . .	22
3.2	Analysis . . . . .	22
3.3	IRAS 16293 . . . . .	22
3.3.1	Observation data . . . . .	22
3.3.2	Results . . . . .	22
3.4	L483 . . . . .	24
3.4.1	Observation data . . . . .	24
3.4.2	Results . . . . .	24
<b>4</b>	<b>Discussion</b>	<b>26</b>
<b>5</b>	<b>Conclusions</b>	<b>27</b>
<b>A</b>	<b>Distribution of methylamine lines contaminated by other molecular line emission in Orion-KL</b>	<b>28</b>
A.1	Integrated intensity maps . . . . .	28
A.2	Channel maps . . . . .	32
<b>Acknowledgments</b>		<b>48</b>
<b>References</b>		<b>49</b>



# Chapter 1

## Introduction

### 1.1 Glycine and methylamine

Methylamine is considered as a precursor of the simplest amino acid glycine. Recent experimental studies have shown several reaction pathways to forming glycine in water containing ices starting from CH<sub>3</sub>NH<sub>2</sub> and CO<sub>2</sub> subjected to high energy electrons (Holtom et al. 2005) or UV radiation (Bossa et al. 2009; Lee et al. 2009). Under similar conditions glycine can decompose to yield methylamine and CO<sub>2</sub> (Ehrenfreund et al. 2001). Interstellar methylamine was first detected toward Sgr B2 at 3.5 cm (Fourikis et al. 1974) and at 3mm (Kaifu et al. 1974). Recently, methylamine has been detected in a spiral galaxy with a high redshift of 0.89 located in front of the quasar PKS 1830-211 (Muller et al. 2011). It was also observed in cometary samples of the Stardust mission (Glavin et al. 2008).

図(??)にメチルアミンの構造を示す。

## 1.2 Star forming region

### 1.2.1 Orion Kleinmann-Low nebula

今回の研究対象としているこの Orion Kleinmann-Low (KL) 天体はオリオン星雲の中にある赤外線星雲であり、太陽からおよそ 437 pc (約 1425 光年) 離れた位置に存在している [21]。この領域では、太陽の 30 倍の質量をもつ巨大な星が誕生している非常に活発な領域であり、広い範囲の周波数を観測する line survey でも数多くの分子が観測されている [5, 22]。この Orion KL は太陽から最も近い位置にある大質量星形成領域であり、放射強度も強く、なおかつ多くの分子が存在するため、この領域に関しては 1967 年に発見されて以来、line survey を含めた多くの研究が今までにもなされている。Orion-KL において、多くの有機分子が存在する領域として Hot core と Compact ridge と呼ばれる場所が知られている。Hot core は暖かく ( $\sim 150$  K)、コンパクト ( $<0.05$  pc) で、密度の高い ( $10^6$  cm $^{-3}$ ) 領域として知られており [23]、Compact ridge も同様に暖かく密度の高い領域であることが分かっている [24]。しかし、化学的な性質は異なっており、Hot core では窒素を含む分子（たとえば、NH<sub>3</sub>、CH<sub>3</sub>CN など）が多く観測される一方で、Compact ridge では酸素を含む分子（たとえば、CH<sub>3</sub>OH、CH<sub>3</sub>OCH<sub>3</sub> など）が多く発見されている [24]。

### 1.2.2 IRAS 16293-2422

### 1.2.3 L483

## 1.3 Radio observation

電波による宇宙空間の観測は、Karl G. Jansky による 1930 年代の初めての宇宙電波の発見、Grote Reber による世界初の電波望遠鏡の作成以来、宇宙空間の観測方法の 1 つとして確立し、また、第 2 次世界大戦中のレーダー技術の進展を受けて大きな進展を遂げている。これ以降、X 線や赤外線などの波長でも観測が行われるようになり、可視光だけではわからない数々の宇宙の不思議を解き明かしている。ただし、

大気による吸収の影響で、全波長のうち地上から観測可能なのは可視光と電波、赤外線の一部となっている。電波の領域では、20 MHz 以下の周波数は電離層を通りず、また高い周波数では大気の酸素や水蒸気に吸収されやすい。このため、電波望遠鏡の設置場所としては、標高が高く、水蒸気が少ない場所が適切である。可視光や赤外線など観測する波長により、宇宙空間で異なる現象を捉える事ができるが、電波による宇宙空間の観測では他の波長にはない特徴がある。・可視光では見えないような低温の物体を観測できる。生まれた後の星は可視光を放射するが、星が生まれる前の温度の低い天体は可視光を放射せず、電波を放射している。そのため、このような天体の研究には電波による観測が必要である。・波長が長いこの特徴のため、星間微粒子による吸収を受けにくく、奥の方まで観測することができる。・電気的に干渉技術が容易干渉計と呼ばれる望遠鏡では複数のアンテナを離して置いて観測し、電波を干渉させることにより高い分解能を得ることができるが、電波領域ではこの方法により他の波長による観測よりも高い分解能を得ている。以上のような特徴により、電波による観測は天文学で重要な位置を占めている。

### 1.3.1 Atacama Large Millimeter Array

## 1.4 Purpose of this work

# Chapter 2

## Methylamine survey in Orion-KL

In this chapter, we report the tentatively detection  $\text{CH}_3\text{NH}_2$  in Orion-KL.

### 2.1 Observation data

We analyzed 2 ALMA archival data. First we used Cycle 2 data (ADS/JAO.ALMA#2013.1.00553.S, Pagani et al. (2017)) We also employed the ALMA Science Verification (SV) data (ADS/JAO.ALMA#2011.0.00009.SV) at band 6 to fill up the missing frequency coverage of Cycle 2 data. Details of each data are summarized in Table 2.1.

Cycle 2 data cube was already calibrated by observers and the reduced data are available on the Internet<sup>1</sup>. Since the SV data contained not only line emission but continuum emission, we subtracted continuum emission statistically by the method described in Section 2.2.1.

---

<sup>1</sup><http://cdsarc.u-strasbg.fr/viz-bin/qcat?J/A+A/604/A32>

**Table 2.1: Summary of Observations**

Date	Window (spw)	Frequency range (GHz)	FWHM (arcsec)	PA (degree)
29–30 December 2014	1	215.145–216.087	$1.8 \times 1.1$	86
	2	216.342–217.279	$1.8 \times 1.1$	84
	3	217.273–218.211	$2.2 \times 1.0$	102
	4	218.204–219.141	$2.2 \times 1.0$	102
	5	219.127–220.064	$1.9 \times 1.0$	95
	6	219.784–220.721	$1.8 \times 1.0$	95
	7	229.757–230.694	$1.4 \times 0.8$	80
	8	230.699–231.636	$2.1 \times 0.9$	102
	9	232.238–233.175	$1.6 \times 1.0$	80
	10	233.470–234.422	$1.6 \times 0.8$	90
	11	235.084–236.021	$1.7 \times 0.9$	95
	12	236.267–237.206	$1.6 \times 0.9$	87
	13	244.834–245.771	$1.6 \times 0.9$	79
	14	245.773–246.710	$1.6 \times 0.9$	79
	15	250.154–251.091	$1.5 \times 0.9$	88
	16	251.079–252.016	$1.3 \times 0.8$	86
20 January 2012	0–16	213.715–246.627	$1.8 \times 1.3$	-1

## 2.2 Analysis

### 2.2.1 Continuum Subtraction of SV data

With the advent of highly sensitive facilities such as ALMA, the spectral lines which were hindered by the noise level with previous telescope can now be detected. Most of these line-rich sources including hot cores are associated with detectable continuum emission. In the analysis of molecular emission lines, the determination and the subtraction of this continuum emission is an essential, but difficult task. Therefore, we improved the method devised in Sanchez-Monge et al. (2017) and deduced continuum subtraction in the observed UV domain (the raw visibilities measured by the interferometer). We introduce the method and results in this section.

## Determination of the continuum level

The determination of the continuum emission level of astronomical sources observed in a spectral line observing mode is based on the identification of channels free of line emission, i.e. line-free channels.

First, we obtain the spectra for which we want to estimate the continuum level. In the case of Orion-KL, many molecular emission exist in Hot core ( $\text{RA}_{J2000} : 05^{\text{h}}35^{\text{m}}14^{\text{s}}.580$ ,  $\text{Dec}_{J2000} : -05^{\circ}22'31''.029$ ) or Compact ridge( $\text{RA}_{J2000} : 05^{\text{h}}35^{\text{m}}14^{\text{s}}.2775$ ,  $\text{Dec}_{J2000} : -05^{\circ}22'30''.776$ ), so we extracted spectra from circular regions with a diameter of  $1''$ .0 with the coordinates indicated by Hirota et al. (2015) as the center. The peak of the distribution is determined over the entire range of the intesity values with a simple symmetric Gaussian fit when assuming the gaussian random error resulting in an estimate of the mean value  $E$  and the standard deviation  $\sigma$ . The width is small in case of pixels with little or no line emission, but for line contaminated regions the distribution becomes broader and the exact location of the peak more uncertain. Subsequently, a skewed Gaussian is fitted to the part of the distribution within  $E - 3\sigma$  and the new centroid (now not necessarily symmetric) is recorded as the continuum level that can then be used for continuum subtraction for that particular pixel.

### 2.2.2 Line identification

We drew  $\text{CH}_3\text{NH}_2$  emission maps using Common Astronomy Software Applications (CASA) software (McMullin et al., 2007). We used JPL Molecular Spectroscopy catalog to identify the transition lines. 8 spectral features exhibit a compact emission at the center of the Hot core . We extracted spectrum from this region. Possible line blending with  $\text{CH}_3\text{NH}_2$  was investigated by JPL database<sup>2</sup>, the Cologne database for molecular spectroscopy (CDMS)<sup>3</sup>, and Splatalogue<sup>4</sup>.

---

<sup>2</sup><http://spec.jpl.nasa.gov>

<sup>3</sup><http://www.astro.uni-koeln.de/cdms/>

<sup>4</sup><http://www.splatalogue.net/>

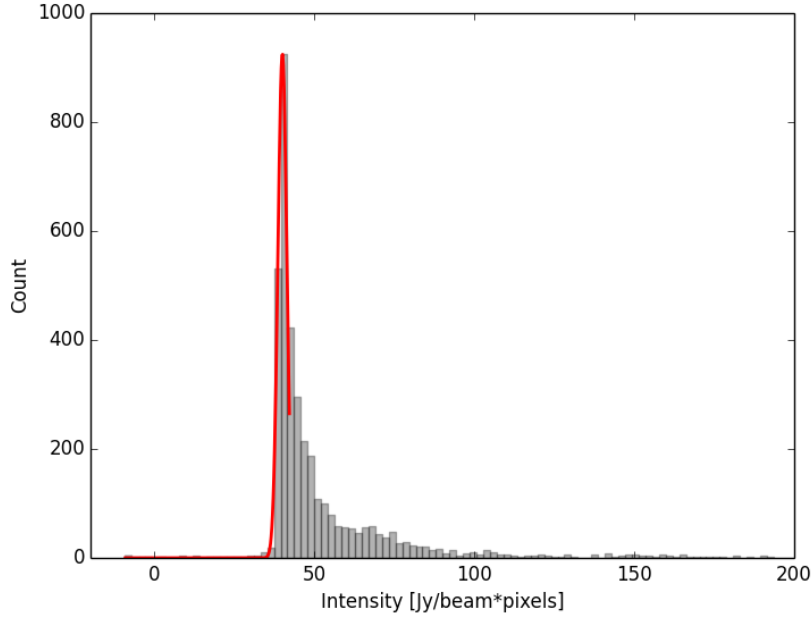


Figure 2.1: Schematic description of the process of determination of the continuum level toward Orion-KL: shown are the flux distributions of Hot core (histogram) with the resulting fit overlaid (red line).

2. We estimated the systemic velocity and the line width of 217.758 GHz line, reported by Pagani et al. (2017), which seem contaminated by other lines.
3. Using these value, we obtained the integrated intensity of 8 transitions described in Table 2.2 by Gaussian fitting.

## 2.3 Results

### 2.3.1 Transitions

The data obtained for  $\text{CH}_3\text{NH}_2$  are summarized in Table 2.2. Here the rest frequencies,  $S\mu^2$ , upper state energy ( $E_u$ ), the quantum numbers, noise level, and peak brightness temperature are given. Out of 32 predicted transitions ( $S\mu^2 > 25 \text{ D}^2$  and  $E_u < 200 \text{ K}$ ) in our observational frequency range, 6 were probably identified in this data set, and are reported in Table 2.2. The remaining 18  $\text{CH}_3\text{NH}_2$  transitions are blended with or masked

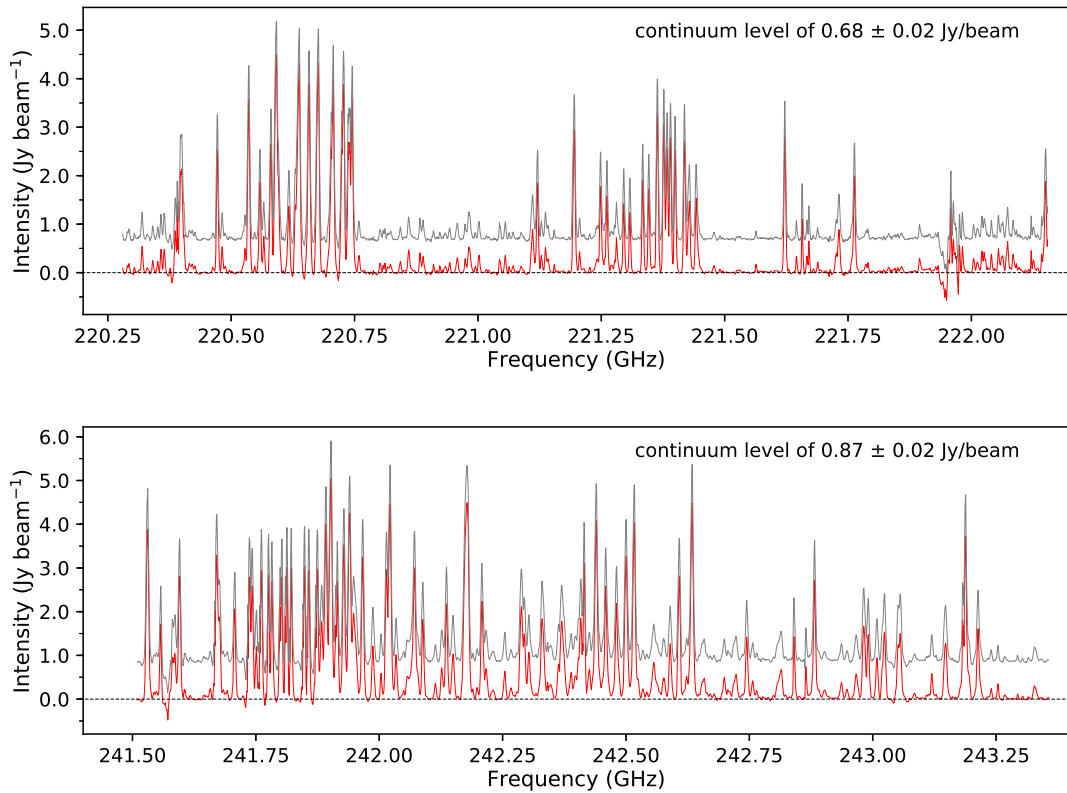


Figure 2.2: The original spectra (gray) and continuum-subtracted spectra (red) towards Hot core. The continuum emission level subtracted to the original spectra, together with its uncertainty, is listed in the upper right part of each panel.

by other spectral features, or its signal are below the noise level (See Appendix A).

**Table 2.2: Observed rotational transitions of  $\text{CH}_3\text{NH}_2$  in Orion-KL**

Frequency [GHz]	$S\mu^2 [\text{D}^2]$	$E_u [\text{K}]$	Transition ( $J, K_a, \Gamma$ )	Noise [K]	peak $T_B [\text{K}]$	Comments
245.202	37.84	168.31	12, 1, $B_2 \rightarrow 11, 2, B_1$			Reported in Pagani+17
217.758	129.88	182.05	12, 2, $B_2 \rightarrow 12, 1, B_1$			Reported in Pagani+17
229.908	27.37	92.71	8, 2, $A_2 \rightarrow 8, 1, A_1$			
235.735	82.06	92.76	8, 2, $B_2 \rightarrow 8, 1, B_1$			Reported in Pagani+17
242.262	60.23	60.86	6, 2, $B_2 \rightarrow 6, 1, B_1$			SV data
244.887	49.54	48.09	5, 2, $B_1 \rightarrow 5, 1, B_2$			Reported in Pagani+17

### 2.3.2 Distribution

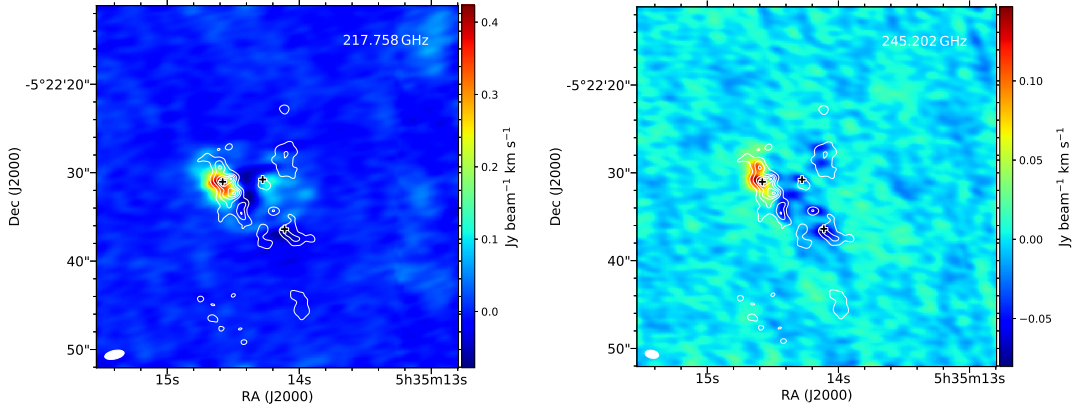


Figure 2.3: Integrated intensity maps of unblended  $\text{CH}_3\text{NH}_2$  lines. The white contours show the 1.3 mm continuum map from Hirota et al. (2015), where the contour levels are 10 %, 30 %, 50 %, 70 %, 90 % of the peak intensity. Black crosses denote Hot core, IRC7, and Compact ridge. The rest frequency of each transition shows in the upper right part of each panel.

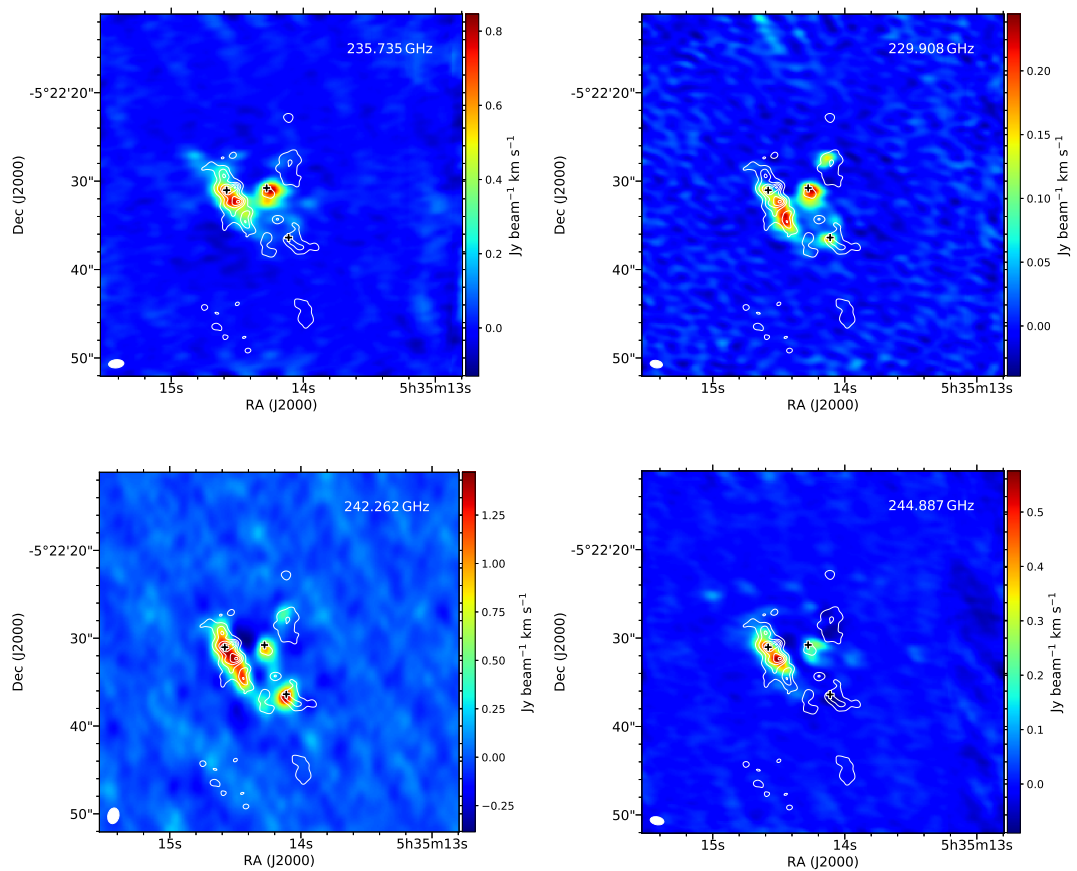


Figure 2.4: (Continued)

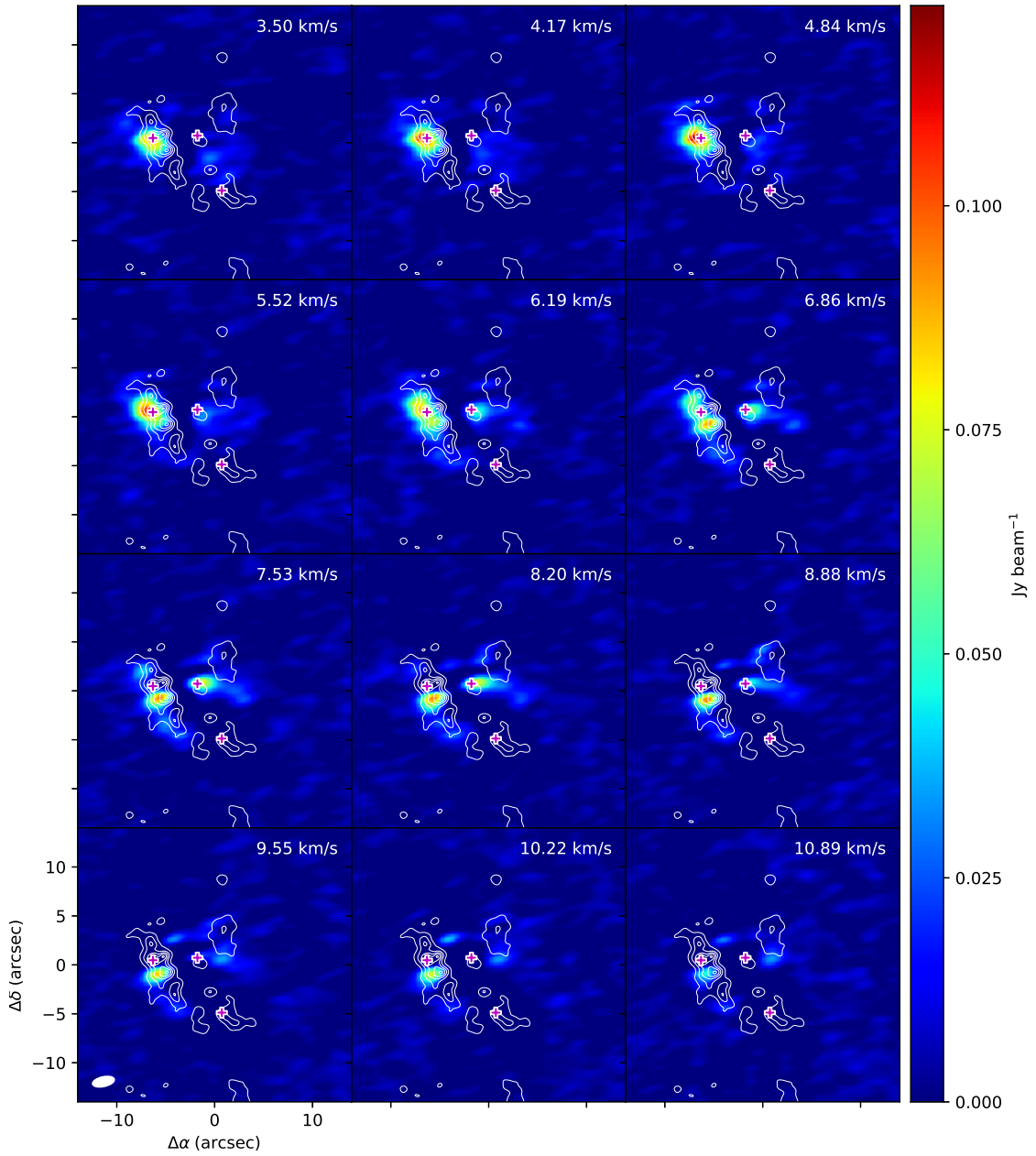


Figure 2.5: Channel map of expected unblended 217.758 GHz line show multiple velocity-dependent emission peaks:  $4\text{-}6 \text{ km s}^{-1}$  towards Hot core,  $7\text{-}9 \text{ km s}^{-1}$  towards IRc7. Magenta crosses denote Hot core, IRc7, and Compact ridge.

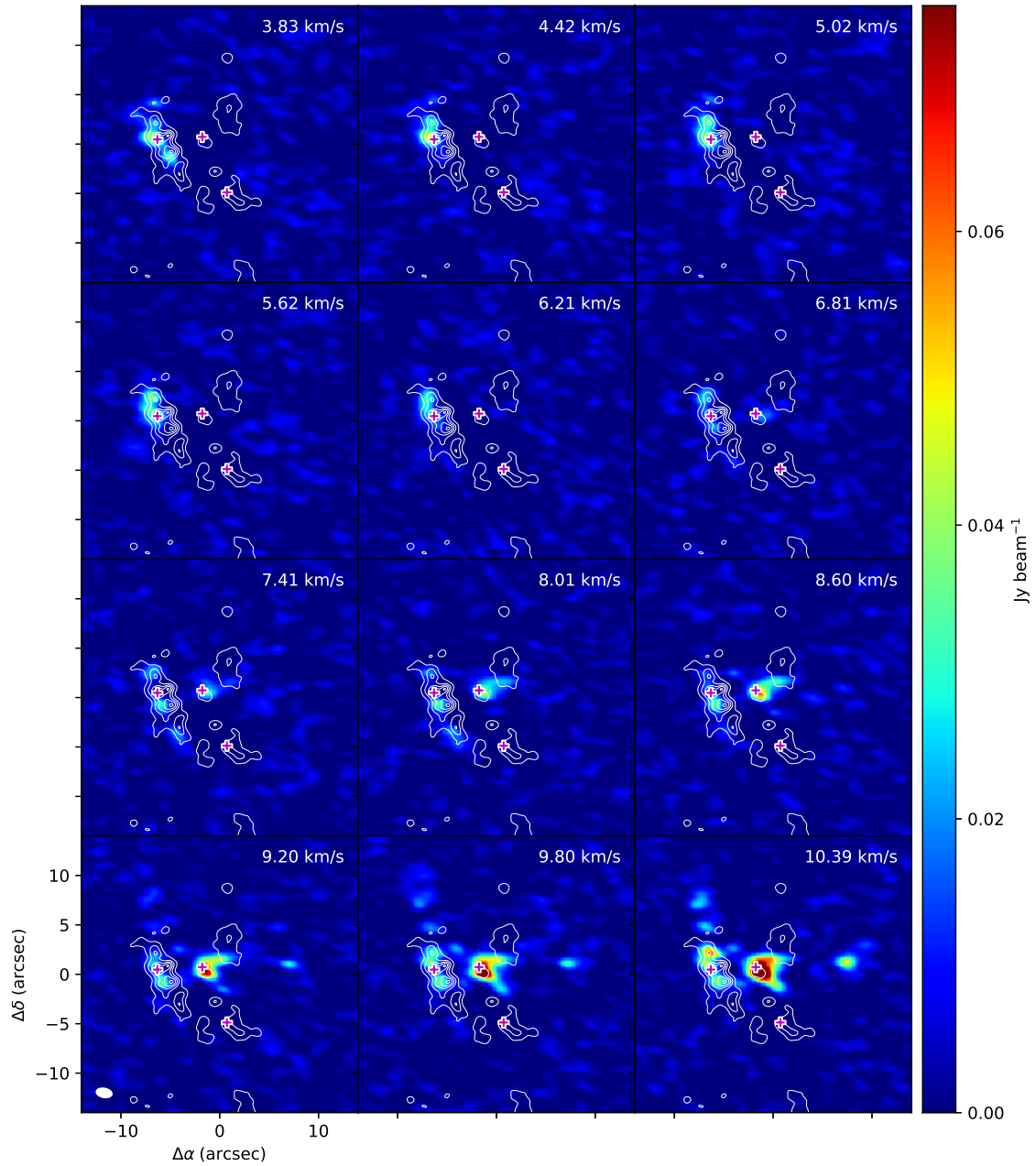


Figure 2.6: Channel map of expected unblended 245.202 GHz line.

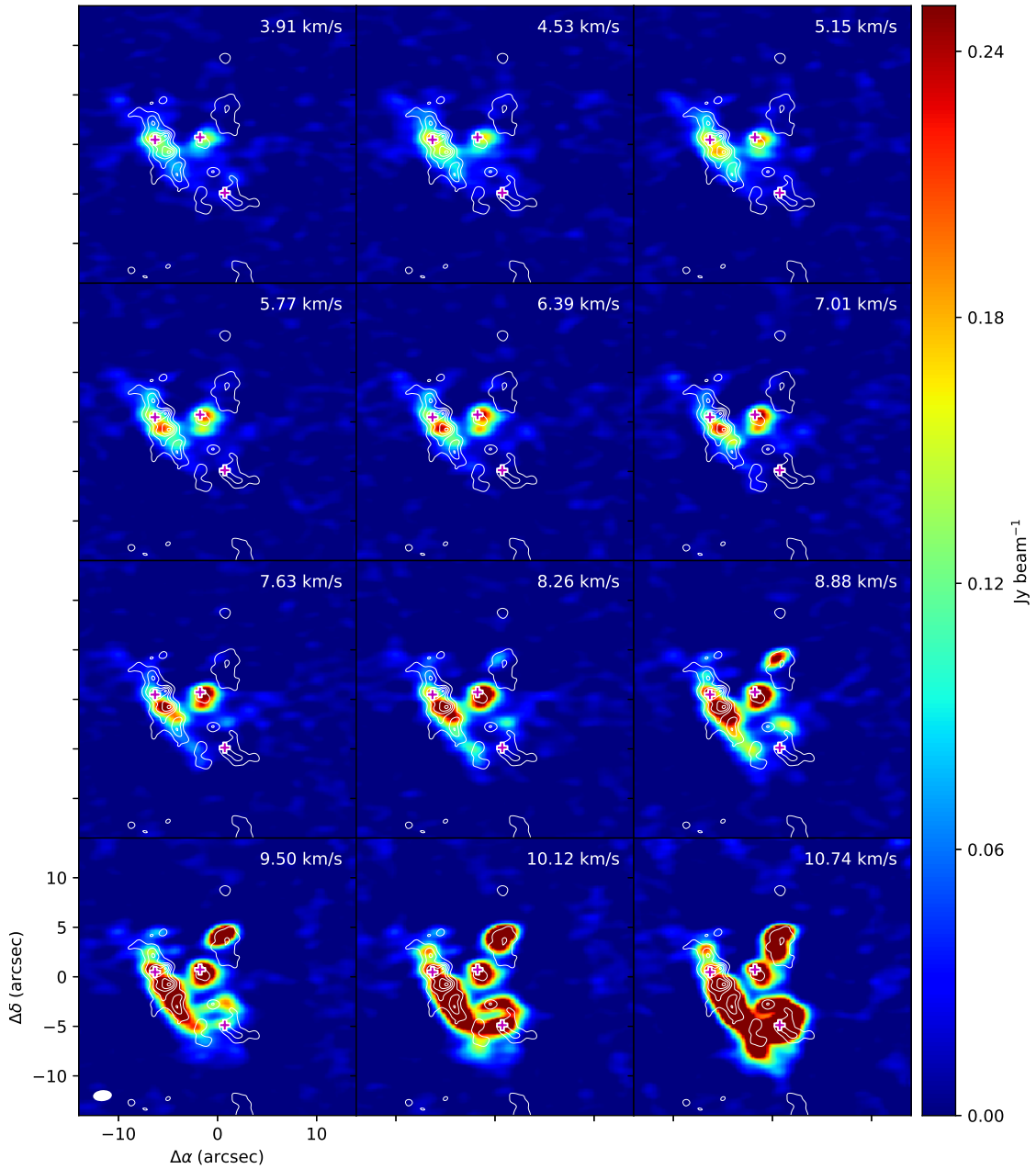


Figure 2.7: Channel map of expected unblended 235.735 GHz line.

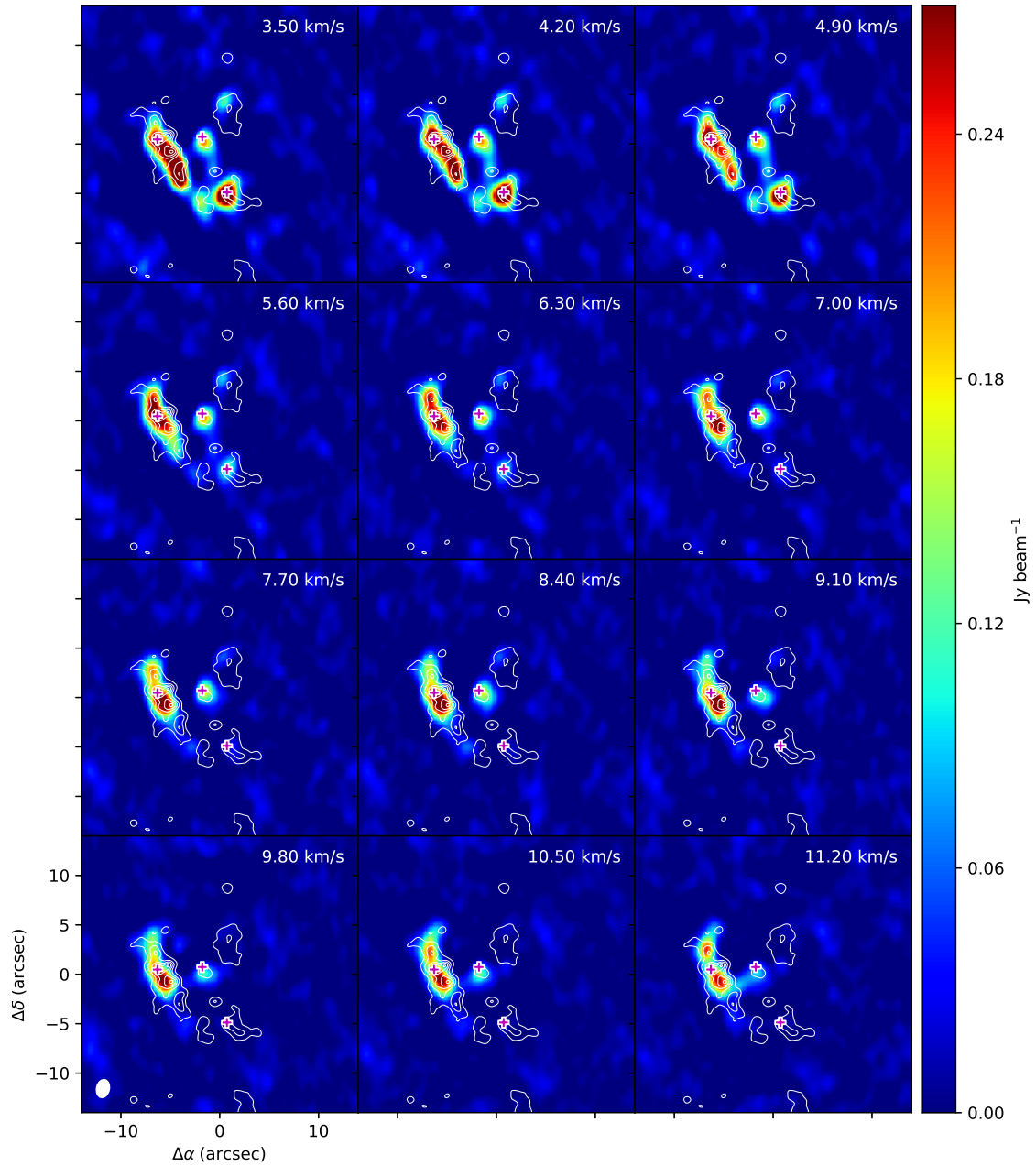


Figure 2.8: Channel map of expected unblended 242.262 GHz line.

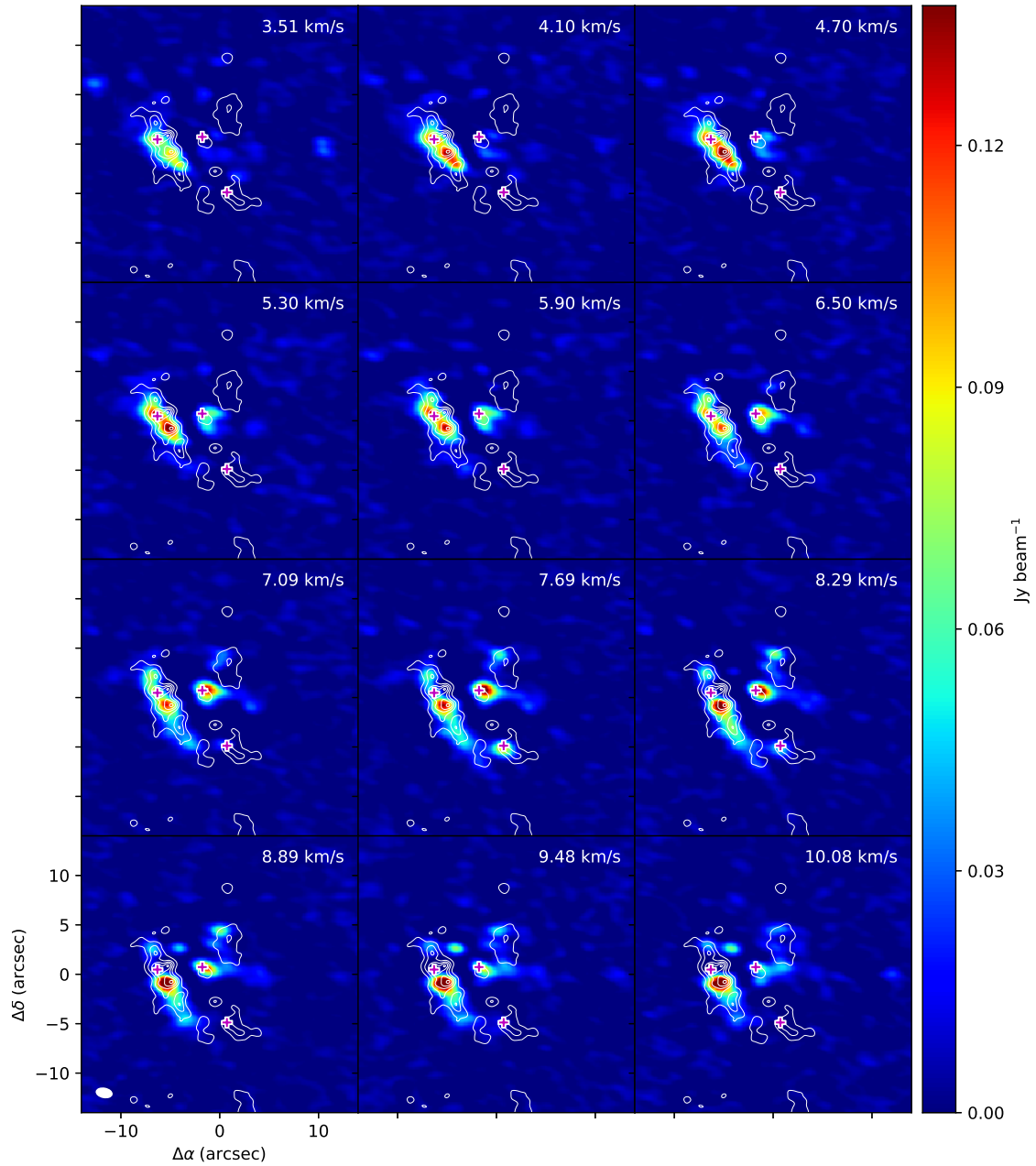


Figure 2.9: Channel map of expected unblended 244.887 GHz line.

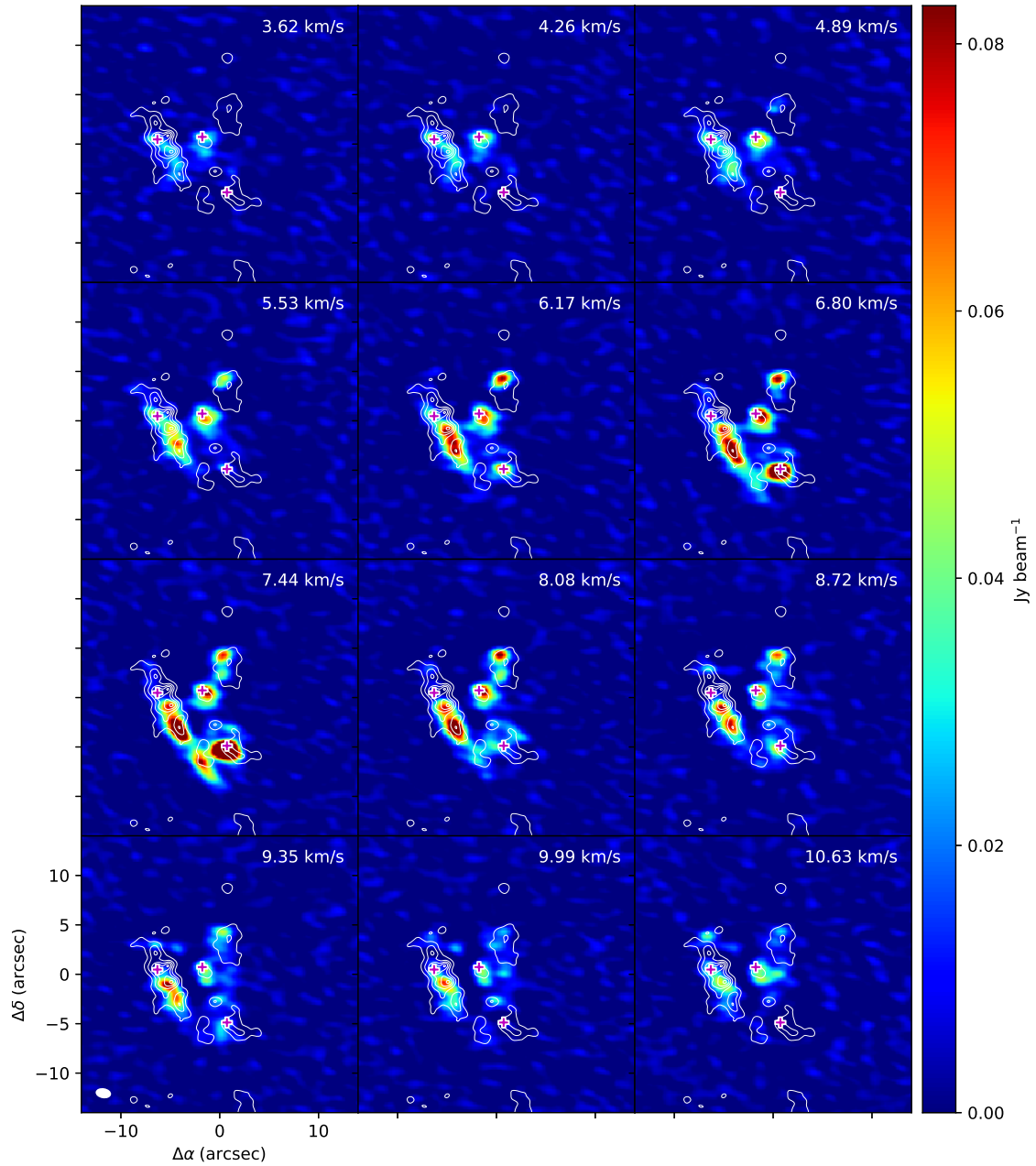


Figure 2.10: Channel map of expected unblended 229.908 GHz line.

### 2.3.3 Spectrum

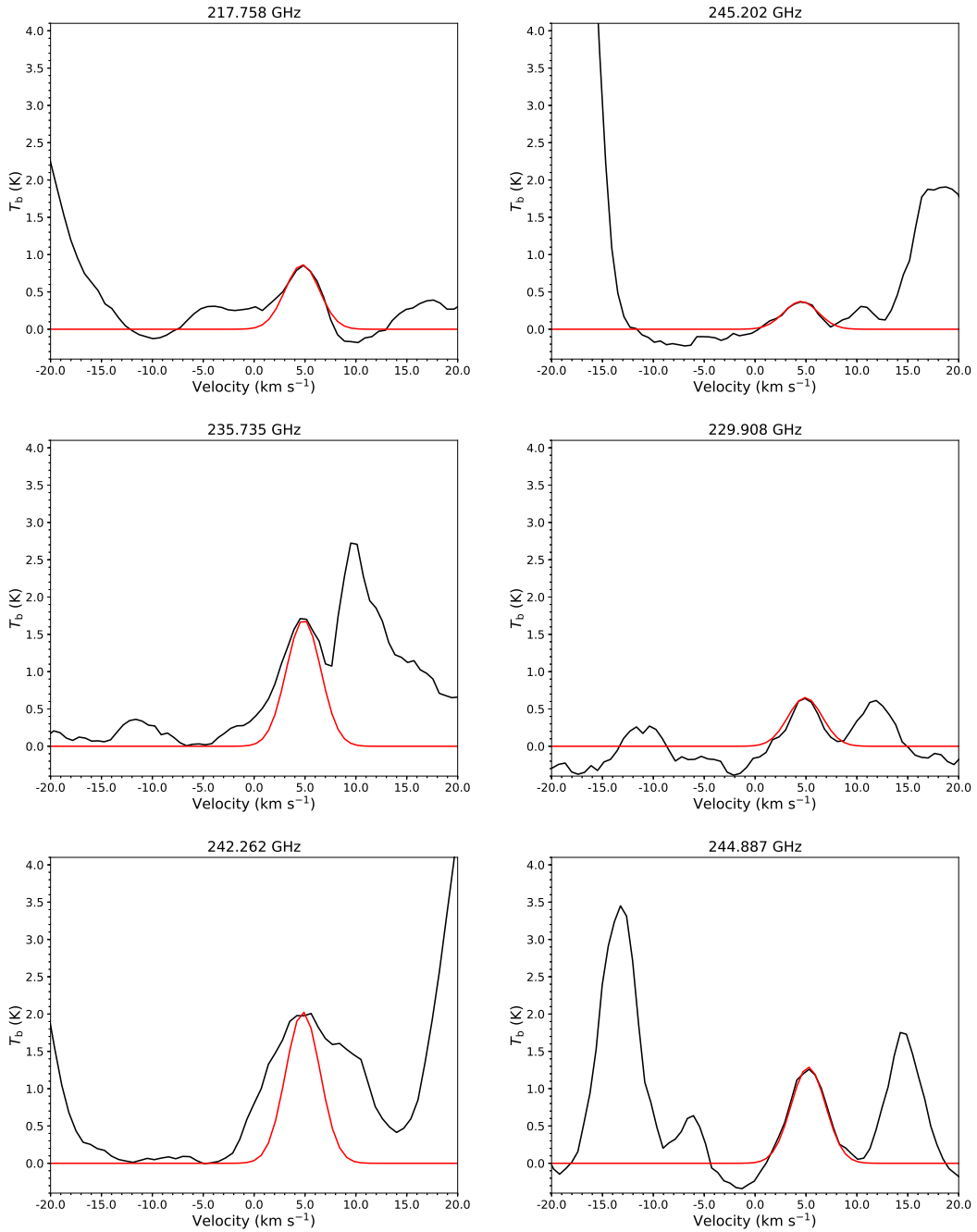


Figure 2.11: Spectrum of the  $\text{CH}_3\text{NH}_2$  lines at each frequency observed in Hot core center (black) and the result of the Gaussian fitting (red).

## 2.4 Disuccion

### 2.4.1 Column density and Rotation temperature

In this subsection we will describe the methodologies in deriving fractional abundances of COMs. The column density of  $\text{CH}_3\text{NH}_2$  ( $N_{\text{MA}}$ ) was established by using the rotational temperature diagram method, which assumes local thermodynamic equilibrium (LTE) and optically thin emission. The following equation was employed for the analysis (Turner, 1991):

$$\log \frac{3 k_{\text{B}} T_{\text{B}} \Delta V_{1/2}}{8 \pi^3 \nu S \mu_0^2} = \log \frac{N_{\text{MA}}}{U_{\text{rot}}} - \frac{E_{\text{u}} \log e}{k_{\text{B}} T_{\text{rot}}} \quad (2.1)$$

In the expression,  $\nu$  is the rest frequency of the transition,  $\mu_0$  is the permanent dipole moment,  $U_{\text{rot}}$  is the rotational partition function,  $S$  is the line strength,  $E_{\text{u}}$  is the upper state energy, and  $T_{\text{B}}$  and  $\Delta V_{1/2}$  are the brightness temperature and line widths (FWHM, in  $\text{km s}^{-1}$ ), respectively. We assumed  $\Delta V_{1/2} = 4.24 \text{ km s}^{-1}$ , which derived by the Gaussian fitting for 217.758 GHz line.

The brightness temperature can be converted from intensity  $I_{\nu}$  when the Rayleigh-Jeans law is applicable.

$$T_{\text{B}} = \frac{c^2}{2 k_{\text{B}} \nu^2} I_{\nu} \quad (2.2)$$

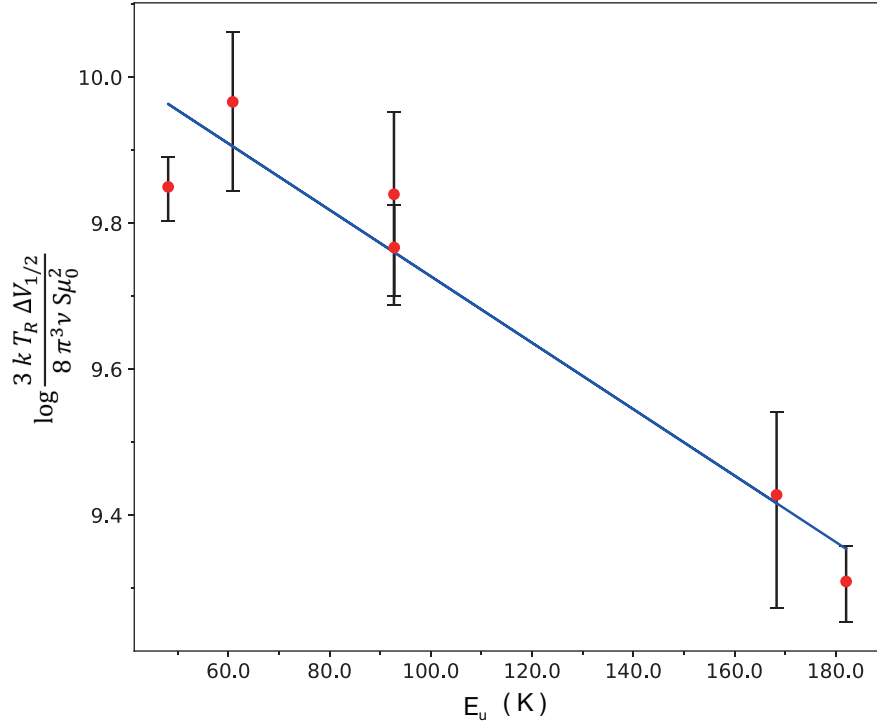


Figure 2.12: Rotation diagram of  $\text{CH}_3\text{NH}_2$  in Hot core. The error bars represents  $\pm 3\sigma$  for each data.

The resulting plots are given in Figure 2.12. The analysis yields a rotational temperature of  $T_{\text{rot}} = 95.4^{+15.5}_{-11.7}$  K, with a column density of  $N_{\text{MA}} = (5.5^{+1.6}_{-1.1}) \times 10^{14} \text{ cm}^{-2}$ .

## 2.4.2 Blending

As shown in Figure 2.13, the  $\text{CH}_3\text{NH}_2$  data produced point-to-point scatter perhaps because of the lower signal-to-noise ratio for the weaker transitions in SV data and possible low-level contamination.

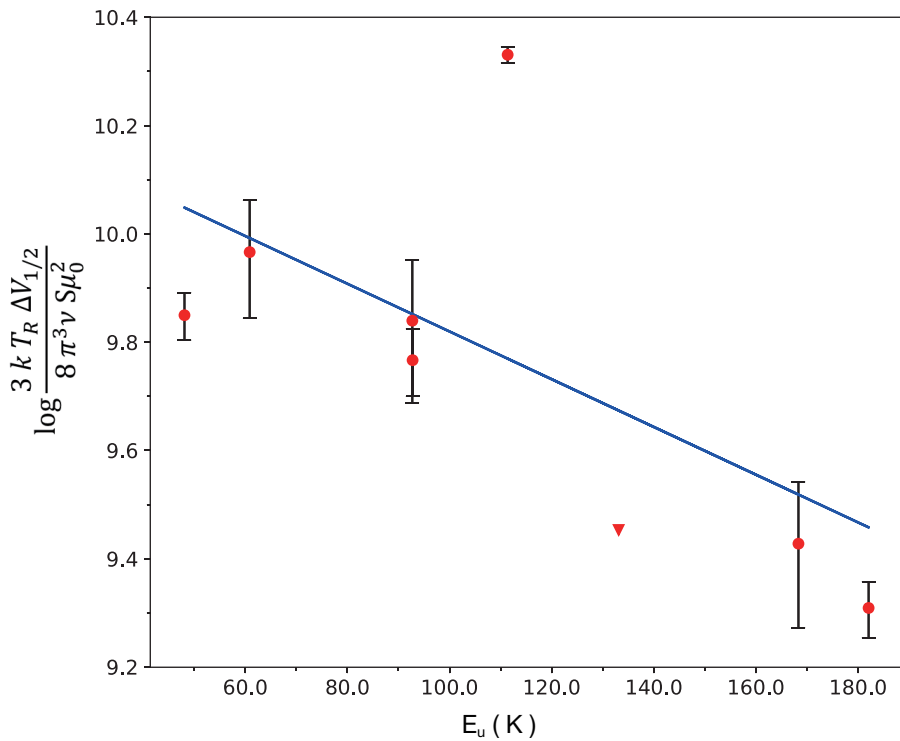


Figure 2.13: Rotation diagram of  $\text{CH}_3\text{NH}_2$  in Hot core with more lines. The error bars represents  $\pm 3\sigma$  for each data. Upper limit is indicated with triangle.



# Chapter 3

## Methylamine survey in low mass star-forming regions

### 3.1 Review of low mass star-forming region

### 3.2 Analysis

### 3.3 IRAS 16293

#### 3.3.1 Observation data

#### 3.3.2 Results

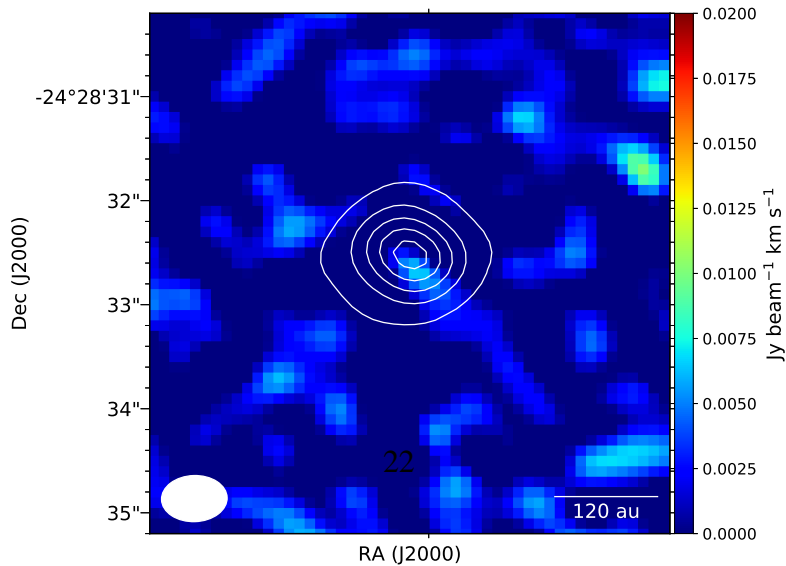


Figure 3.1: Integrated intensity map around 247.362 GHz. The white contours represent

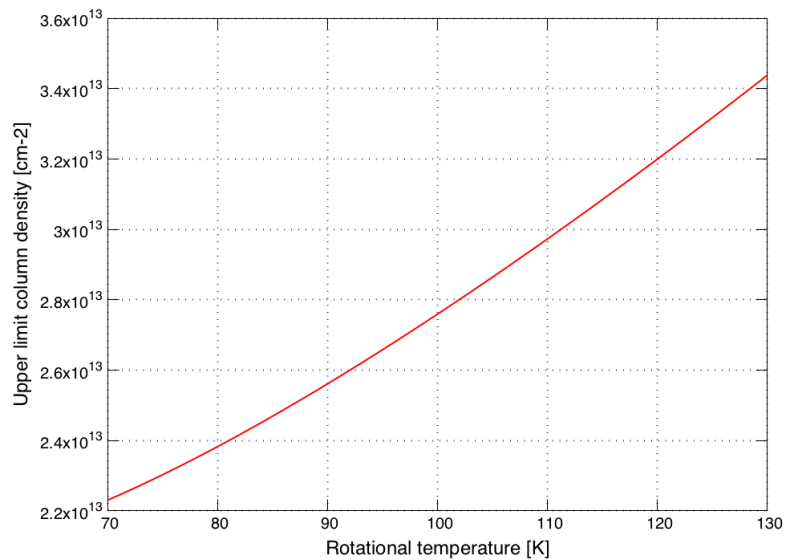


Figure 3.2: Upper limit column density for the strongest  $\text{CH}_3\text{NH}_2$  transition ( $7_2E_{1-1} \rightarrow 7_1E_{1-1}$ ) as function of  $T_{\text{rot}}$ . A  $3\sigma$  value of  $11.4 \text{ mJy beam}^{-1}$  is used.

## 3.4 L483

### 3.4.1 Observation data

### 3.4.2 Results

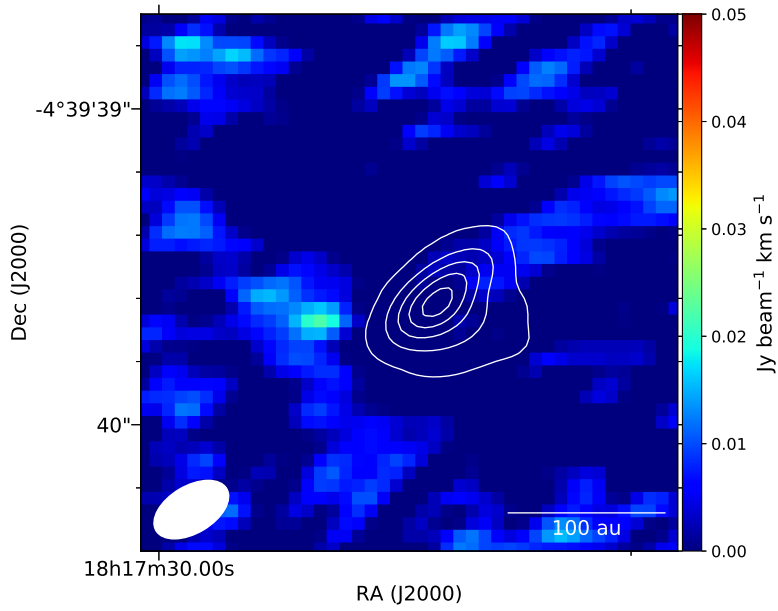


Figure 3.3: Integrated intensity map around 217.079 GHz. The white contours represent the 1.3 mm continuum map, where the contour levels are 10 %, 30 %, 50 %, 70 %, 90 % of the peak intensity.

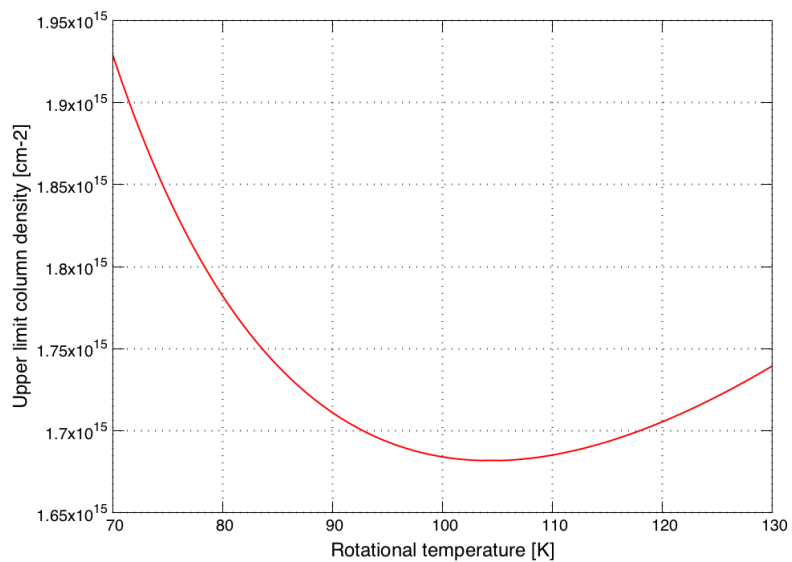


Figure 3.4: Upper limit column density for the strongest  $\text{CH}_3\text{NH}_2$  transition ( $11_2A_1 \rightarrow 11_2A_2$ ) as function of  $T_{\text{rot}}$ . A  $3\sigma$  value of  $22.5 \text{ mJy beam}^{-1}$  is used.

# **Chapter 4**

## **Discussion**

# **Chapter 5**

## **Conclusions**

# **Appendix A**

## **Distribution of methylamine lines contaminated by other molecular line emission in Orion-KL**

### **A.1 Integrated intensity maps**

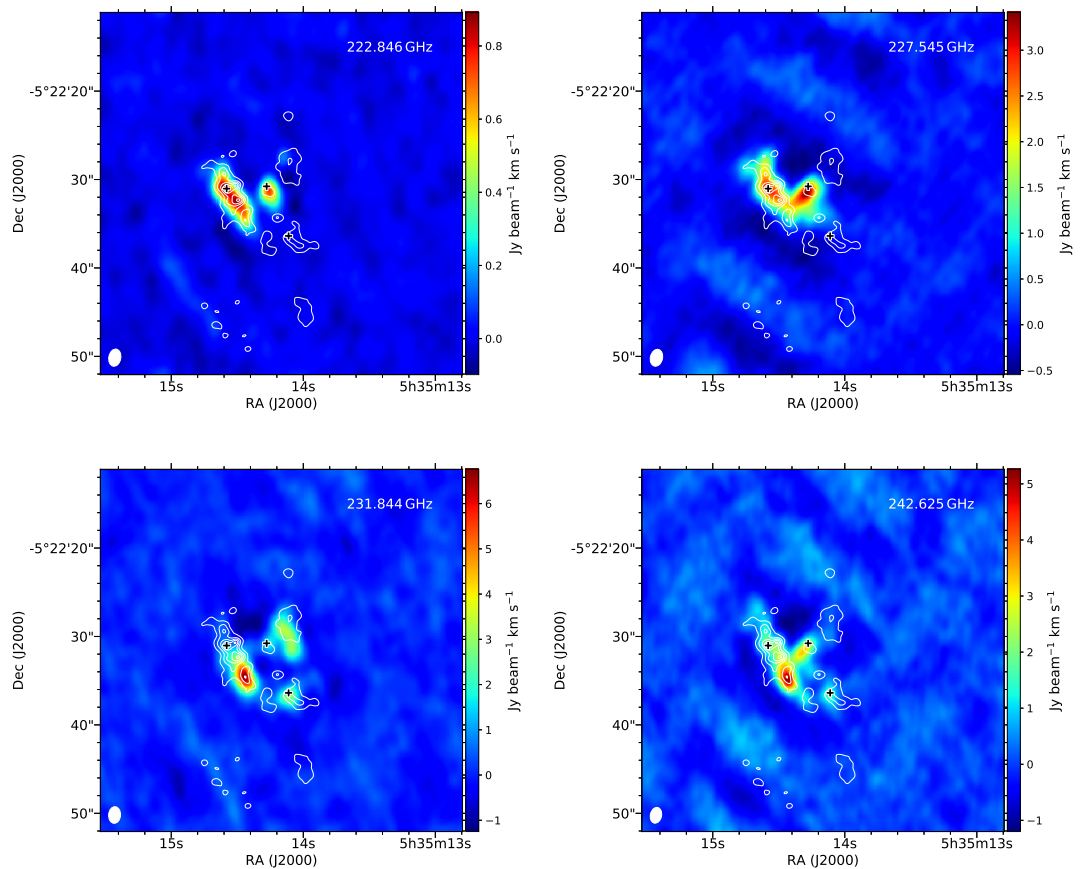


Figure A.1: Integrated intensity maps around methylamine line.

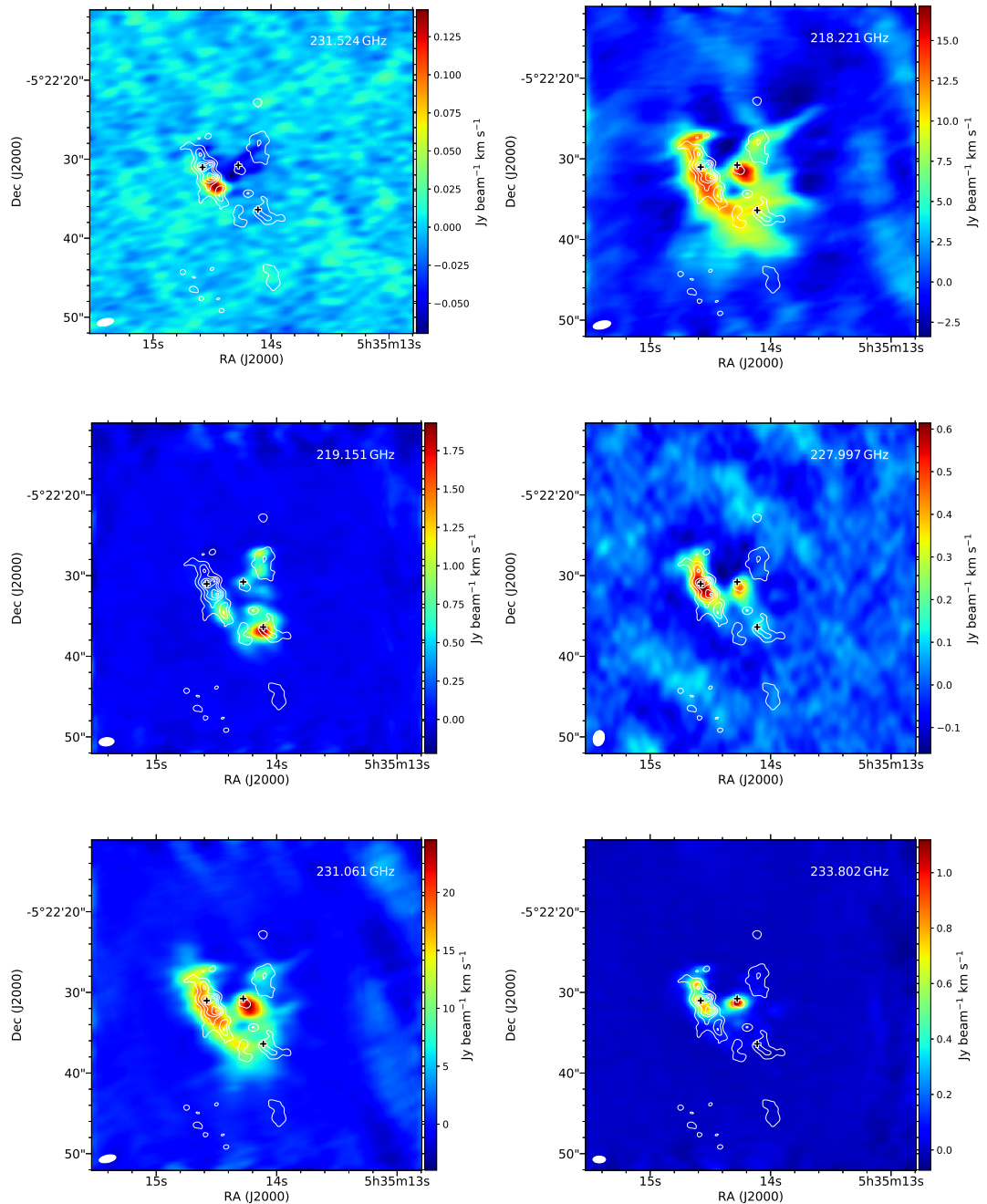


Figure A.2: (Continued)

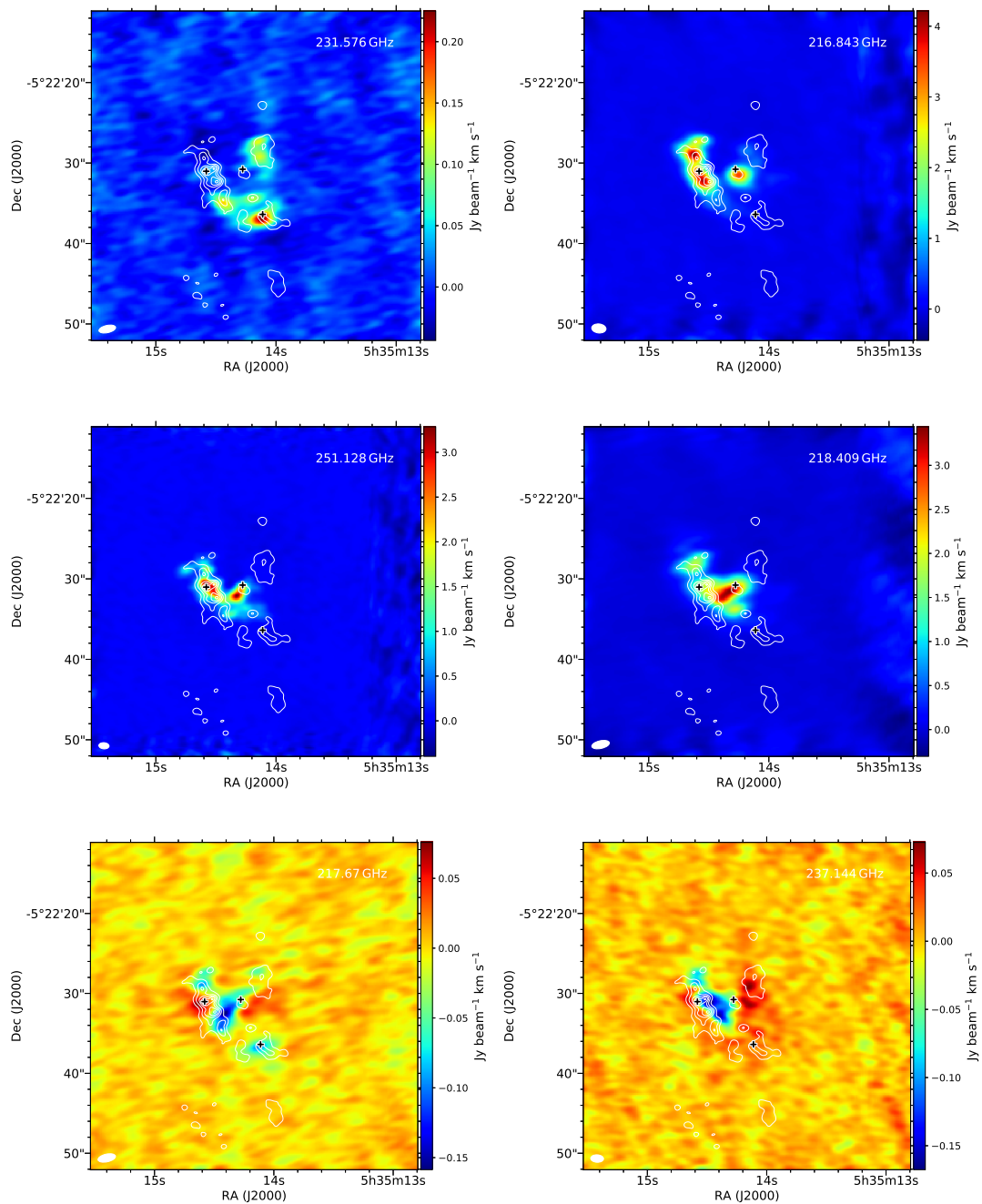


Figure A.3: (Continued)

## A.2 Channel maps

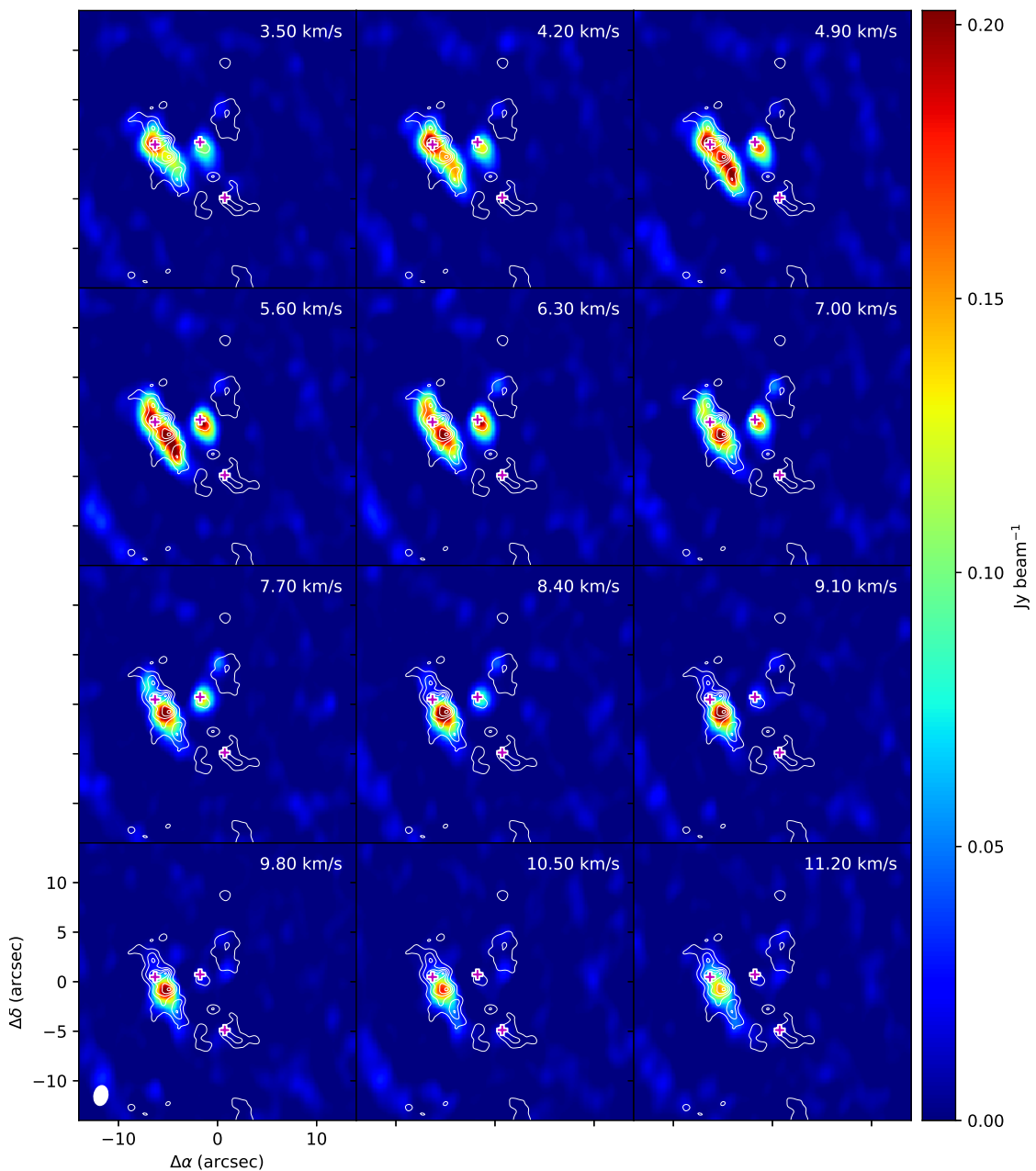


Figure A.4: 222.846GHz

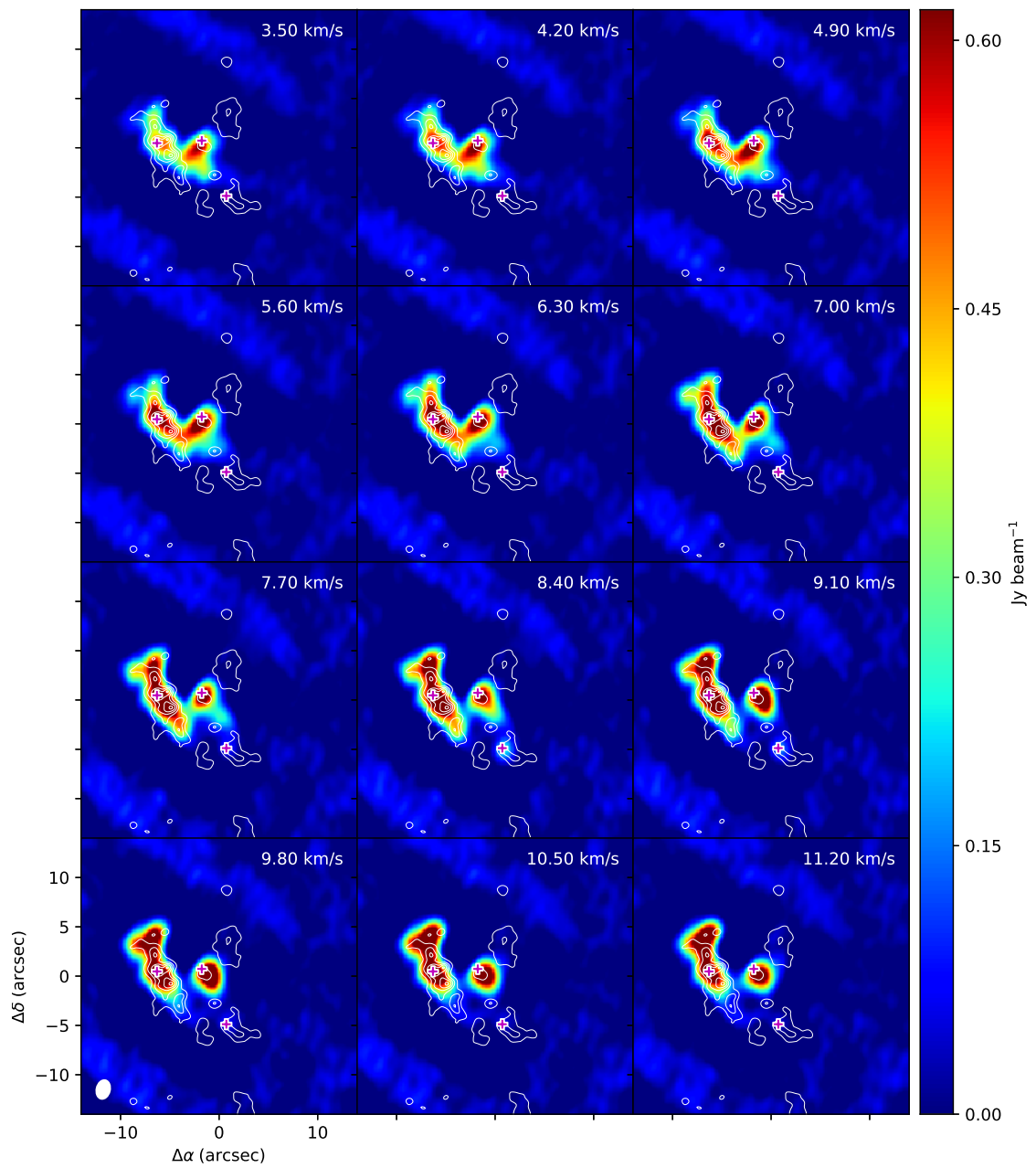


Figure A.5: 227.545GHz

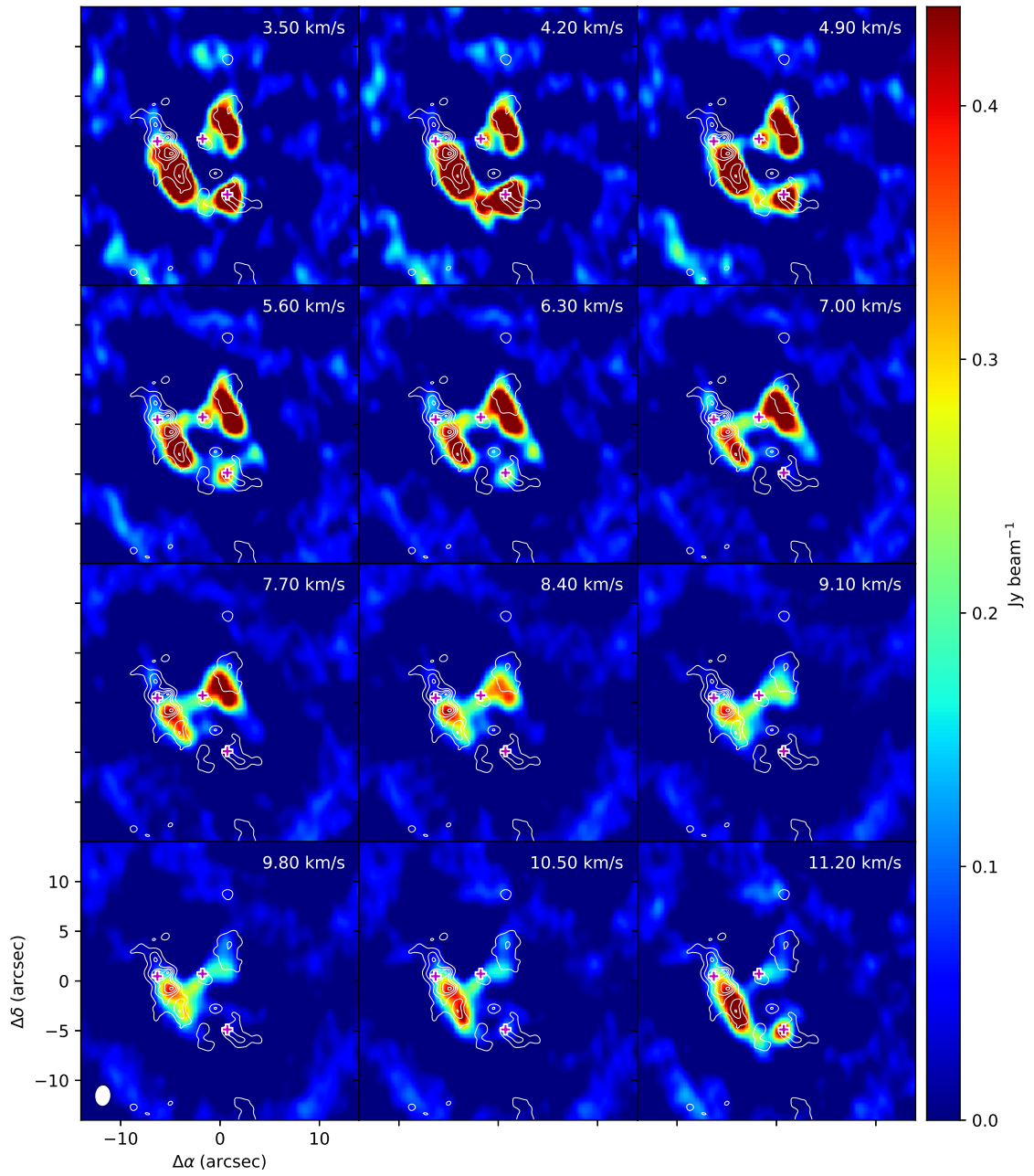


Figure A.6: 231.844GHz

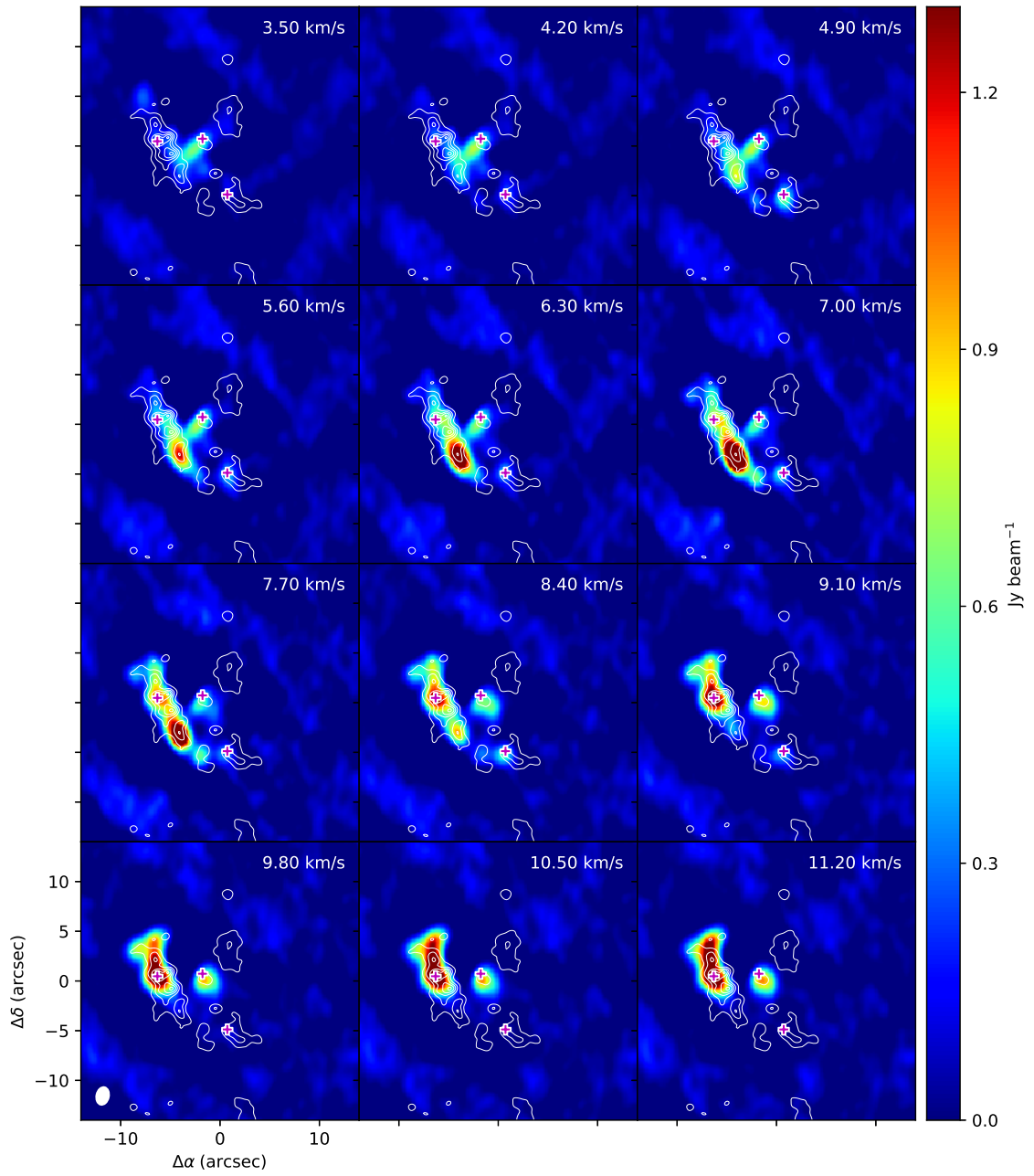


Figure A.7: 242.625GHz

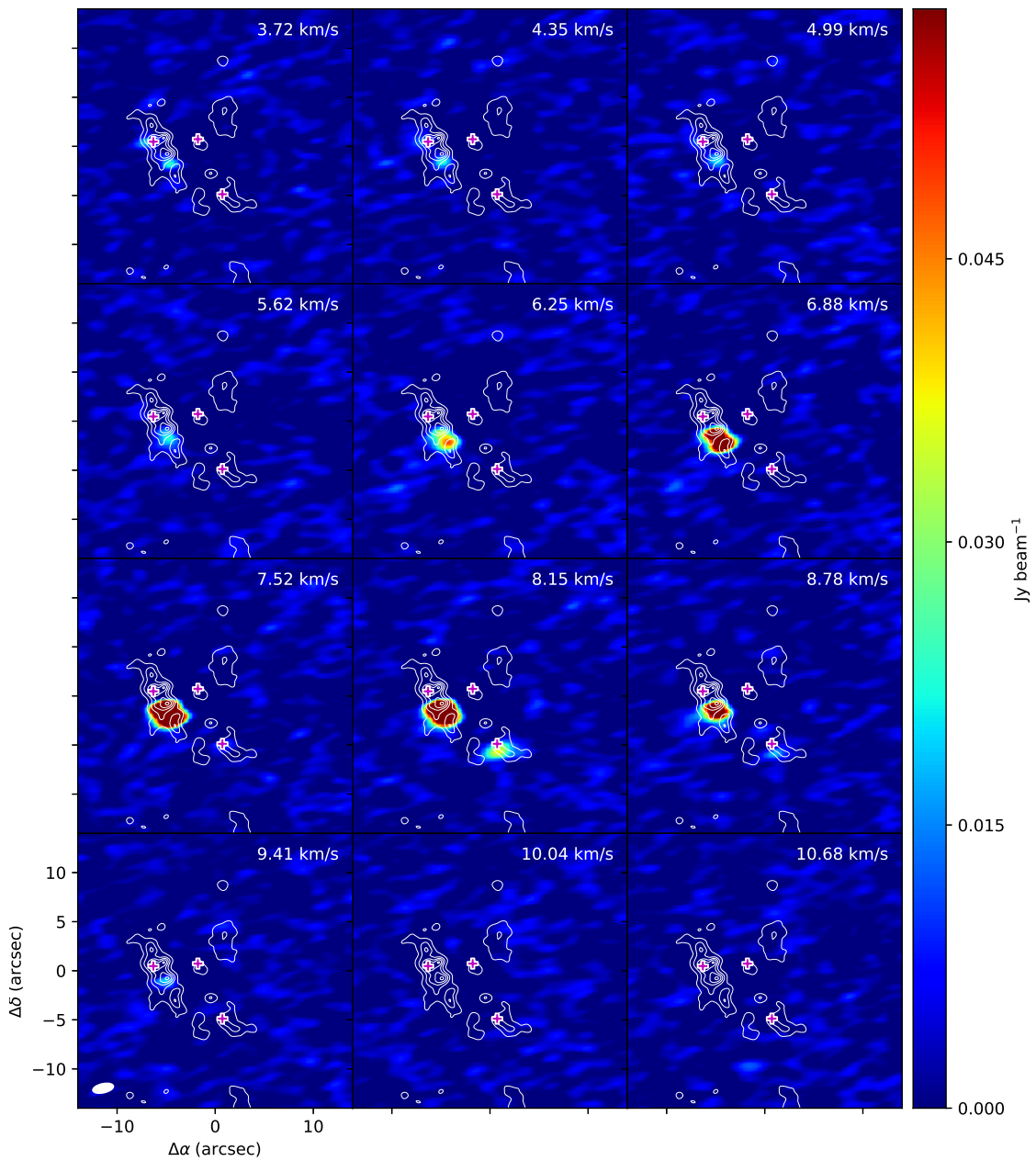


Figure A.8: 231.524GHz

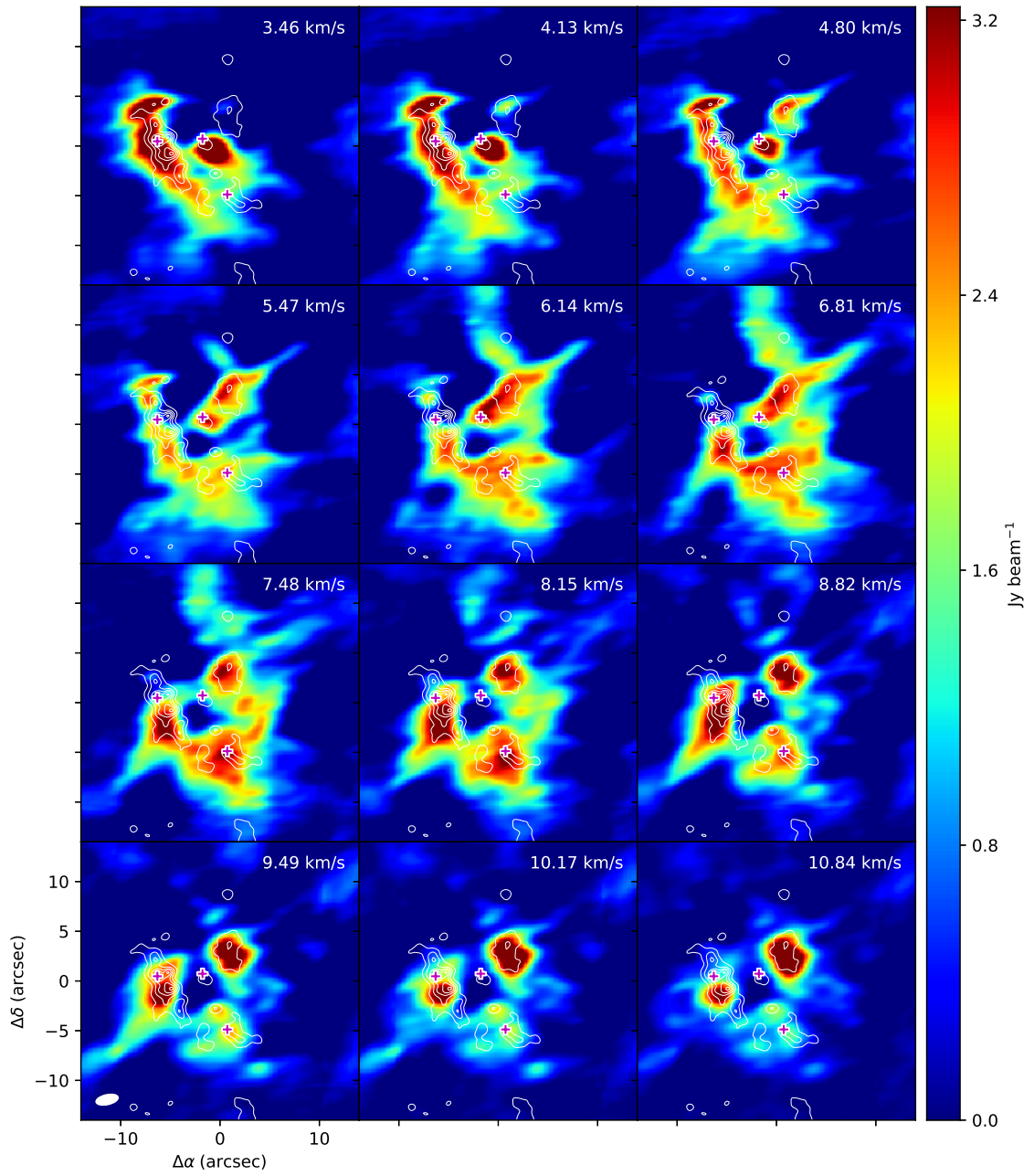


Figure A.9: 218.221GHz

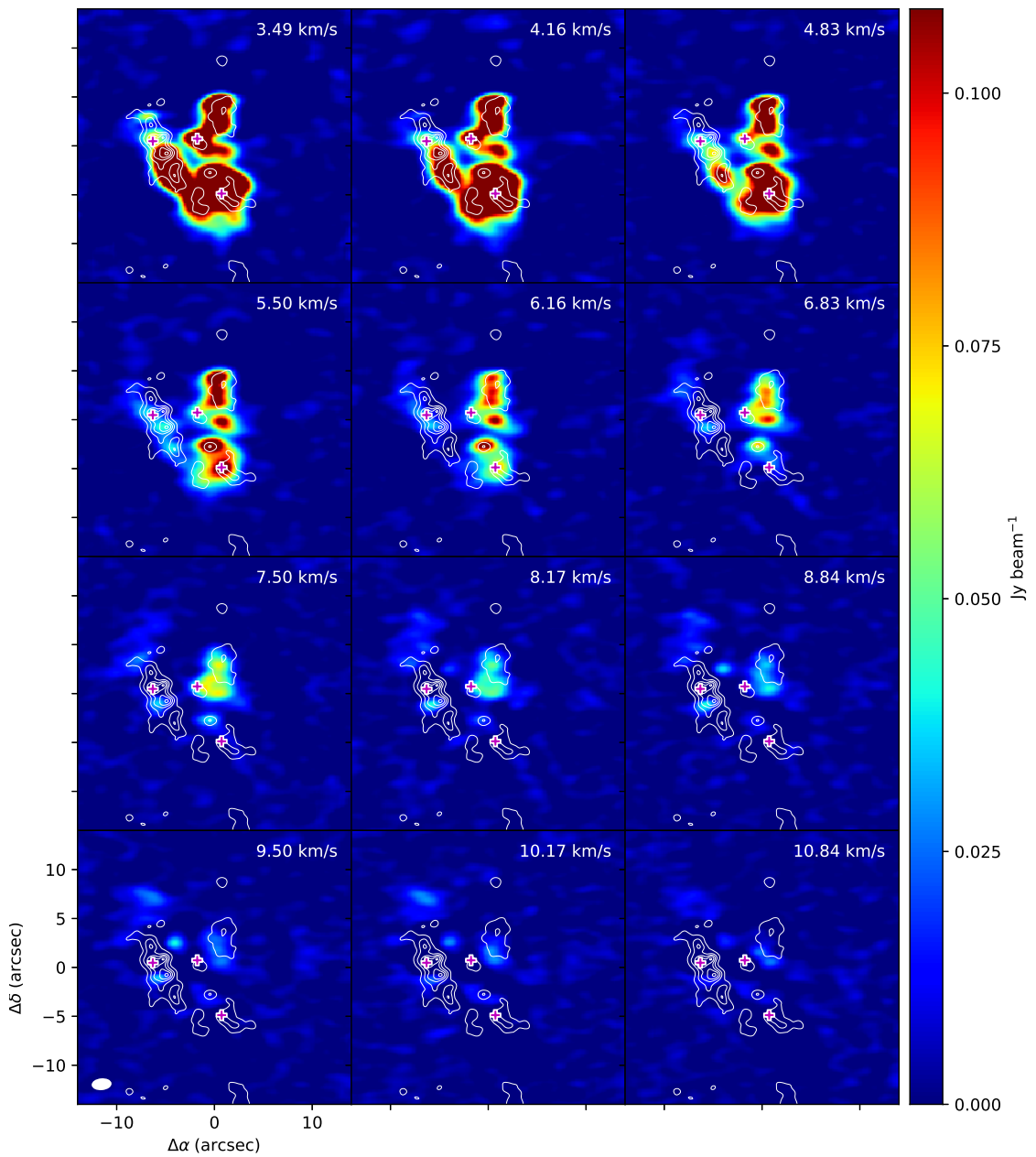


Figure A.10: 219.151GHz

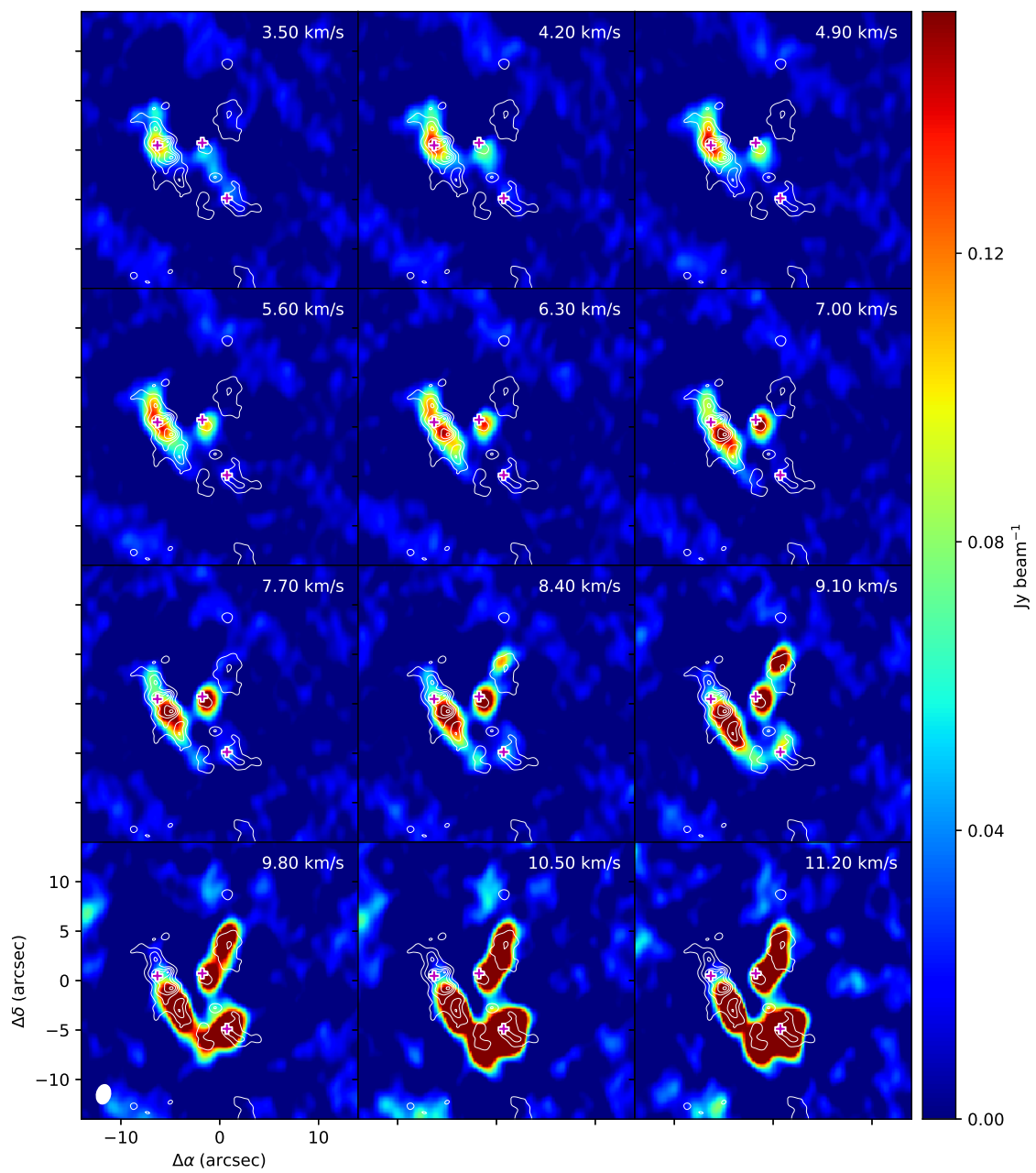


Figure A.11: 227.997GHz

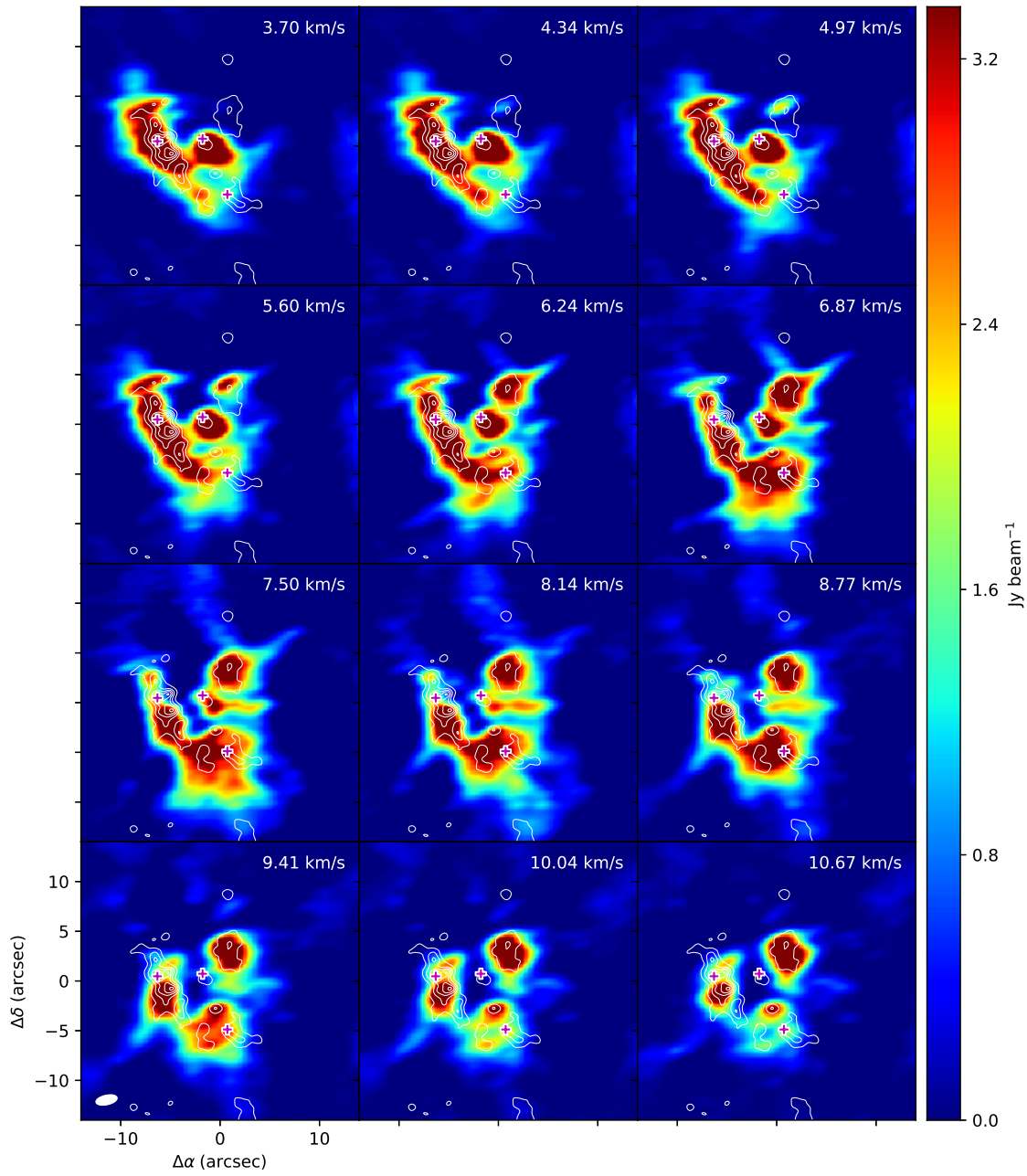


Figure A.12: 231.061GHz

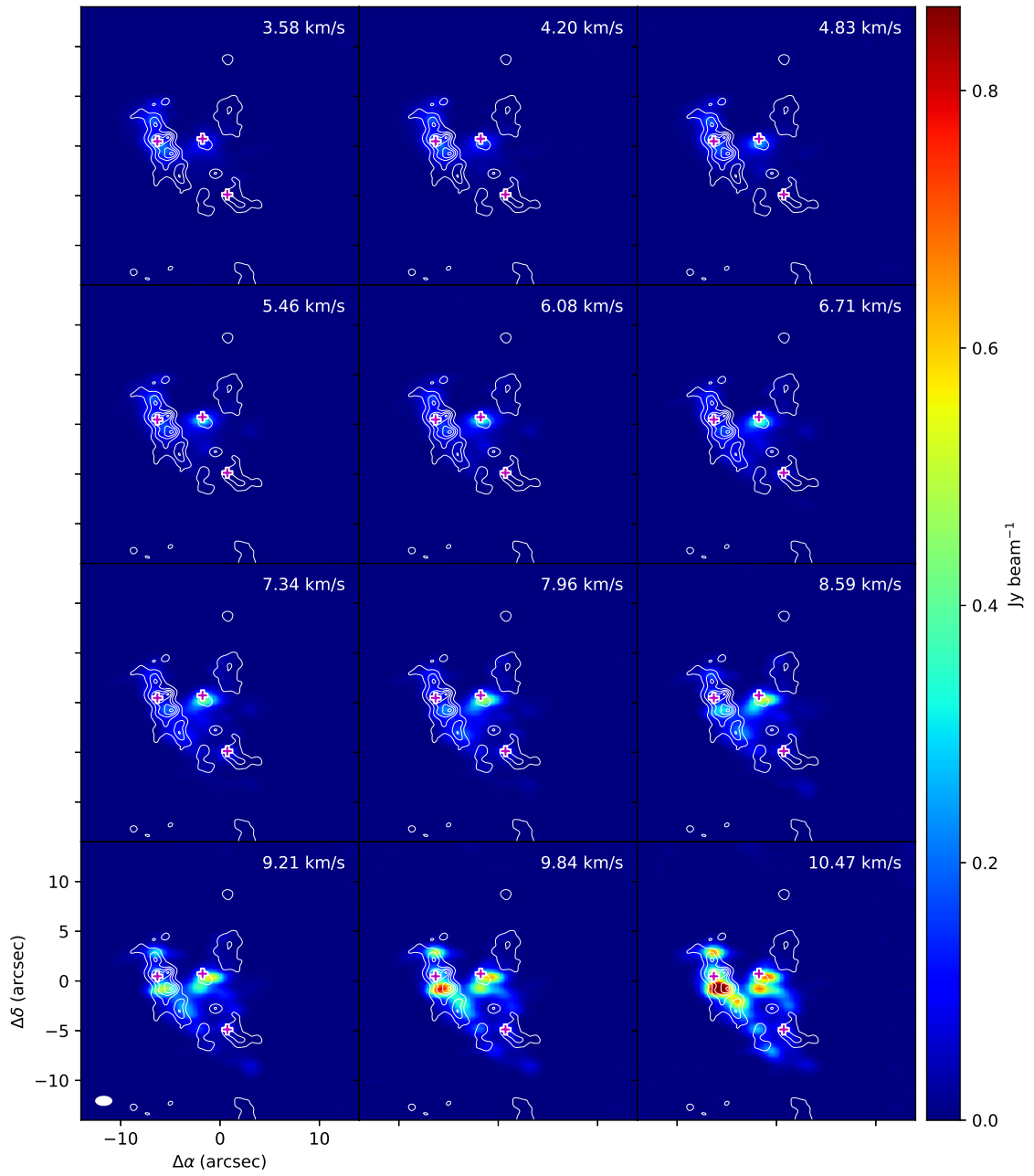


Figure A.13: 233.802GHz

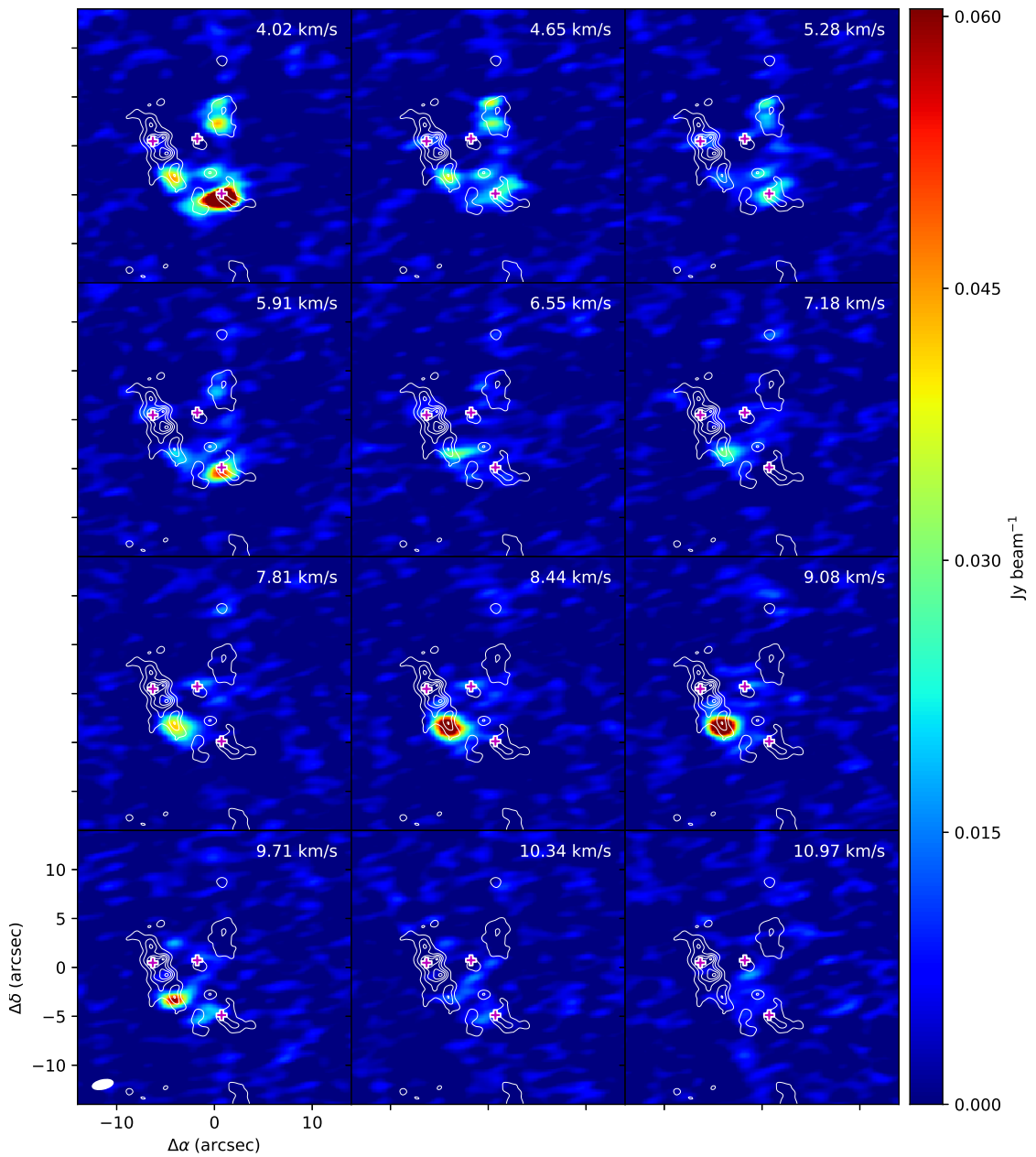


Figure A.14: 231.576GHz

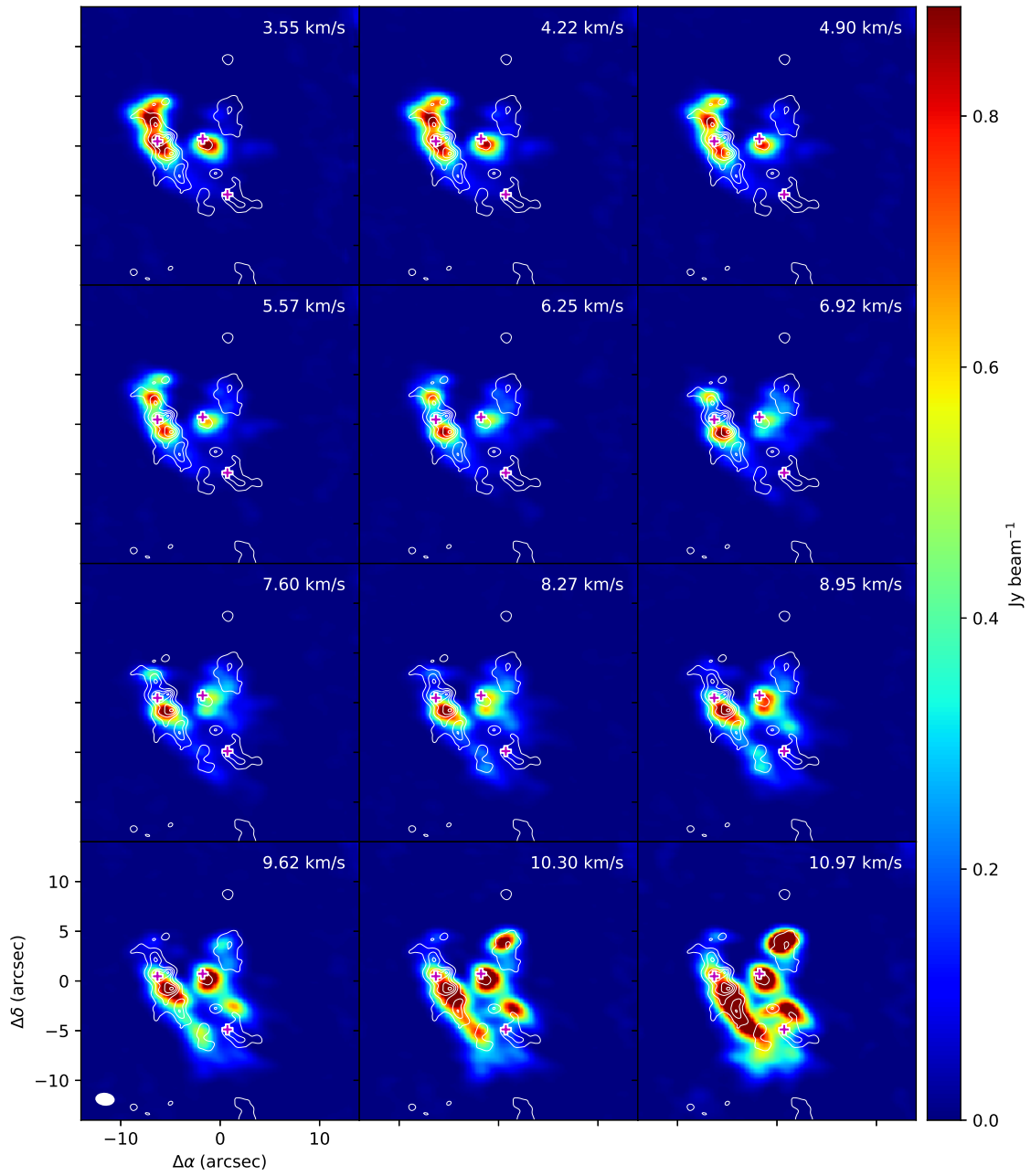


Figure A.15: 216.843GHz

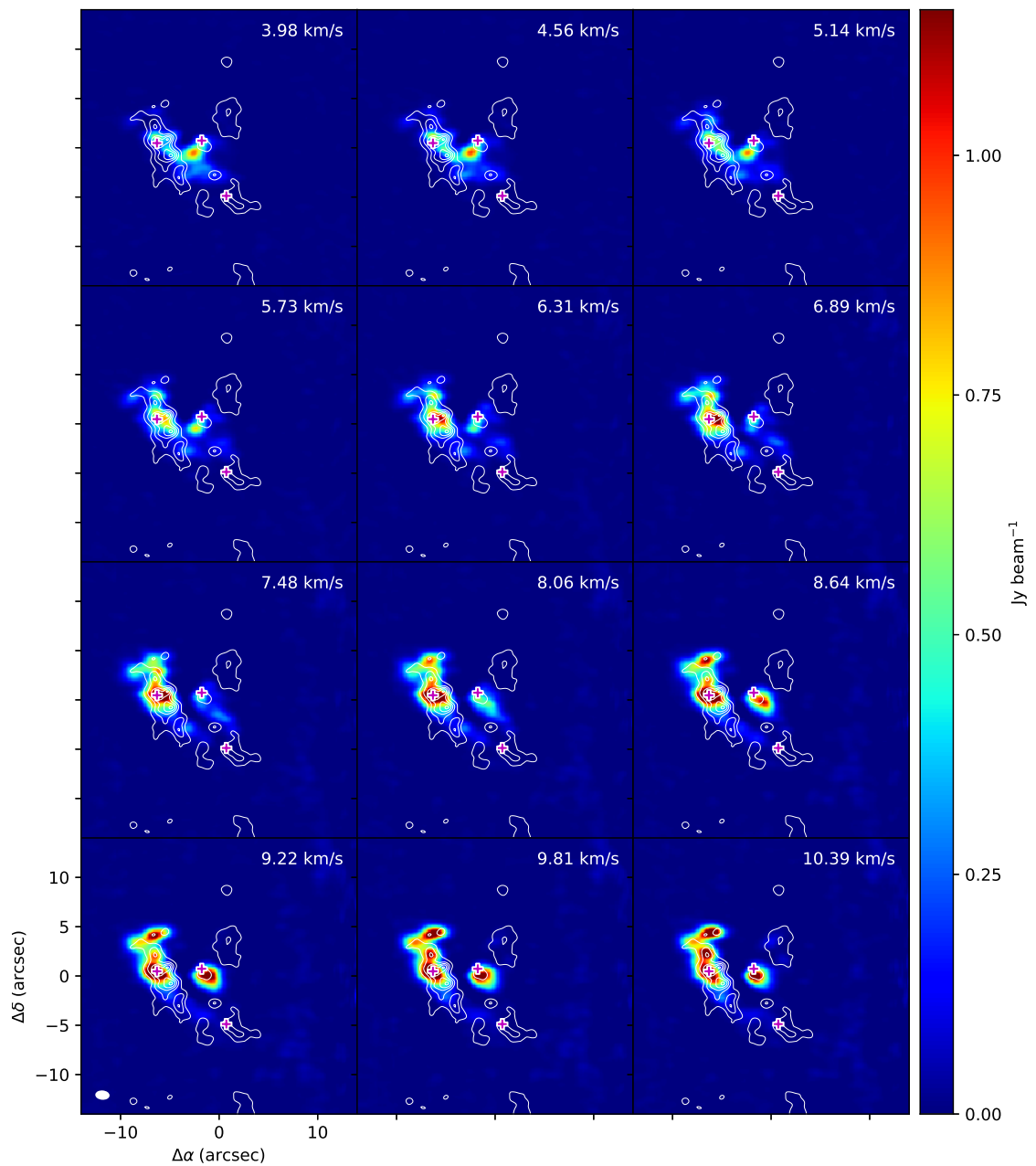


Figure A.16: 251.128GHz

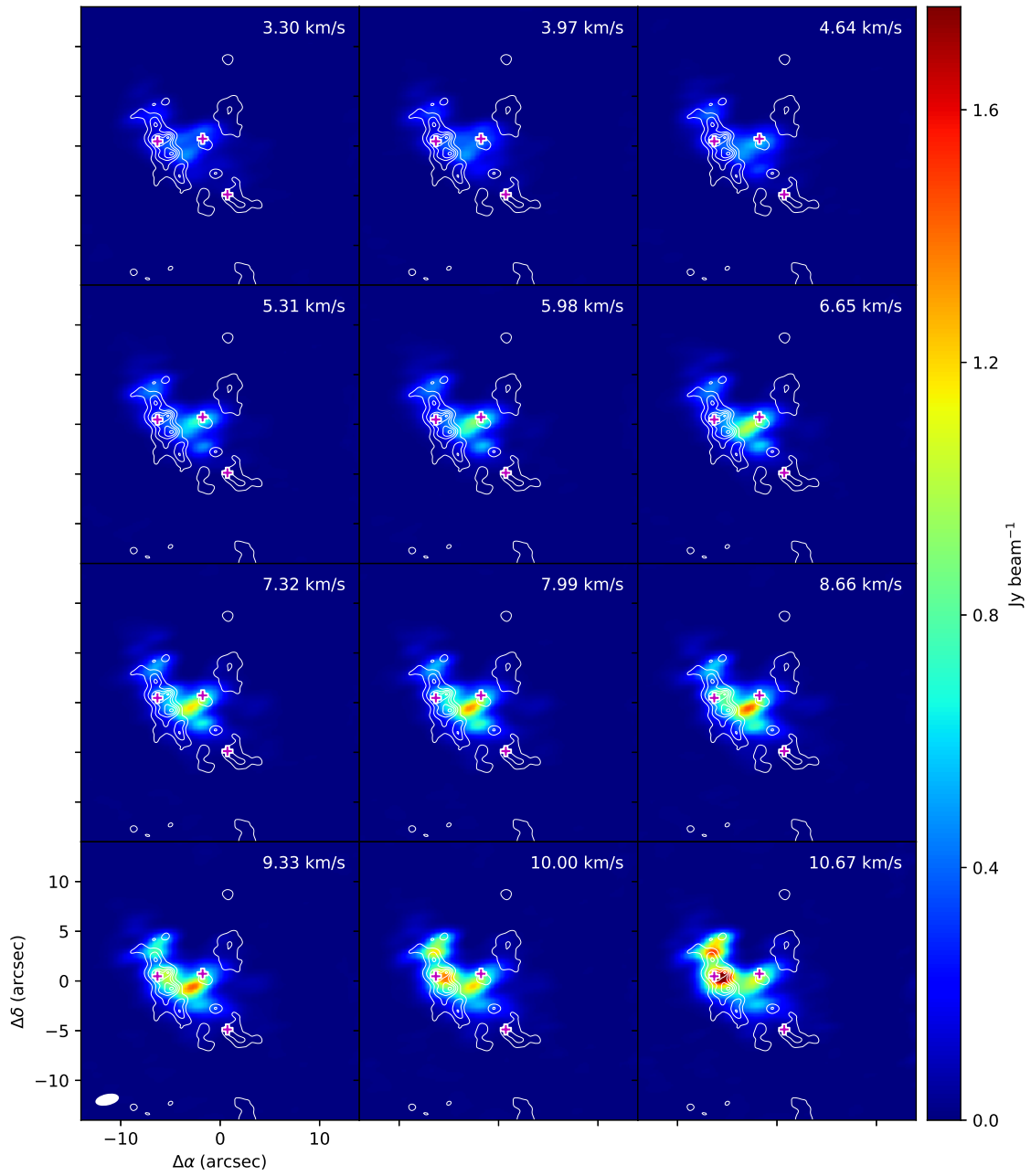


Figure A.17: 218.409GHz

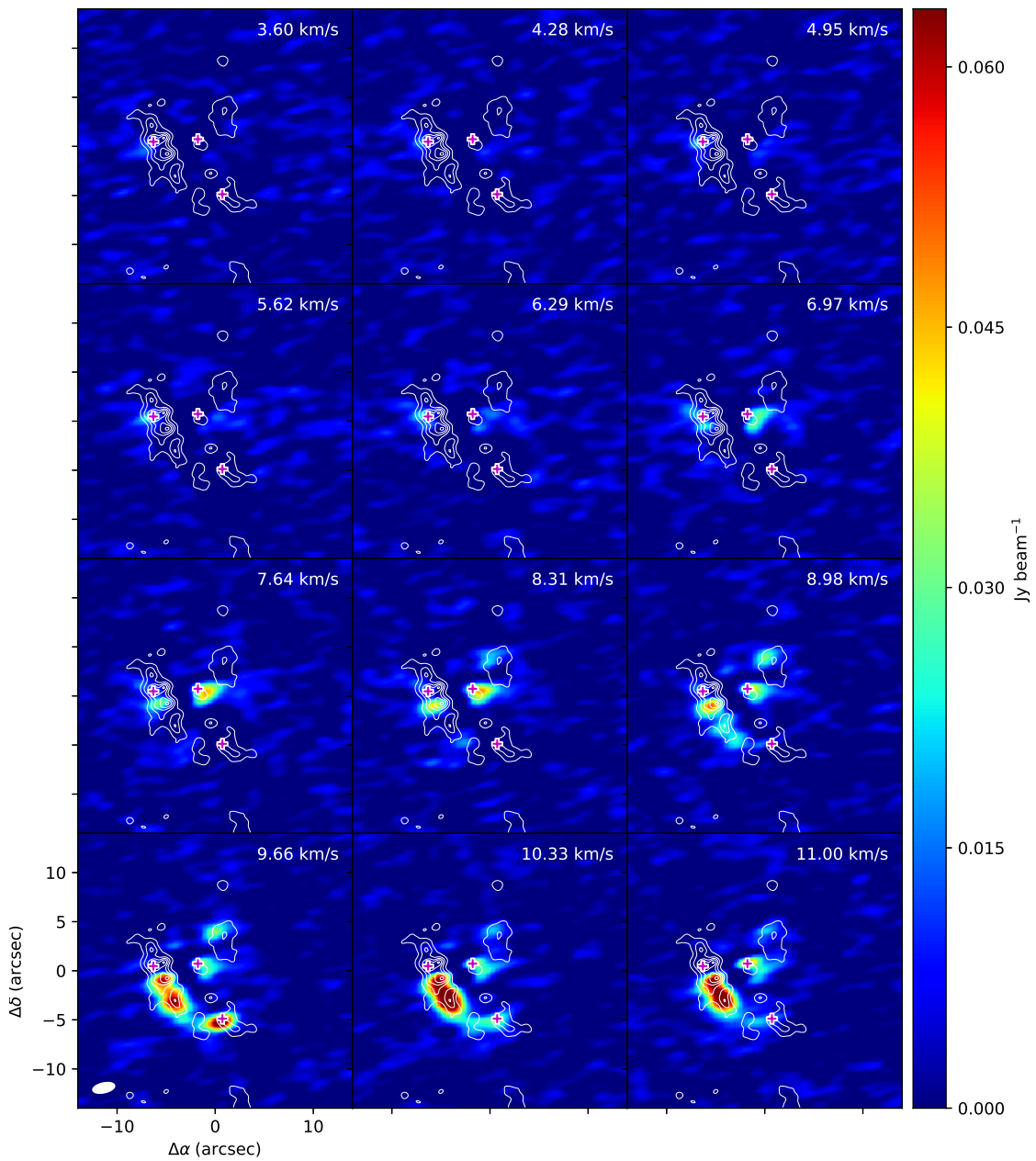


Figure A.18: 217.670GHz

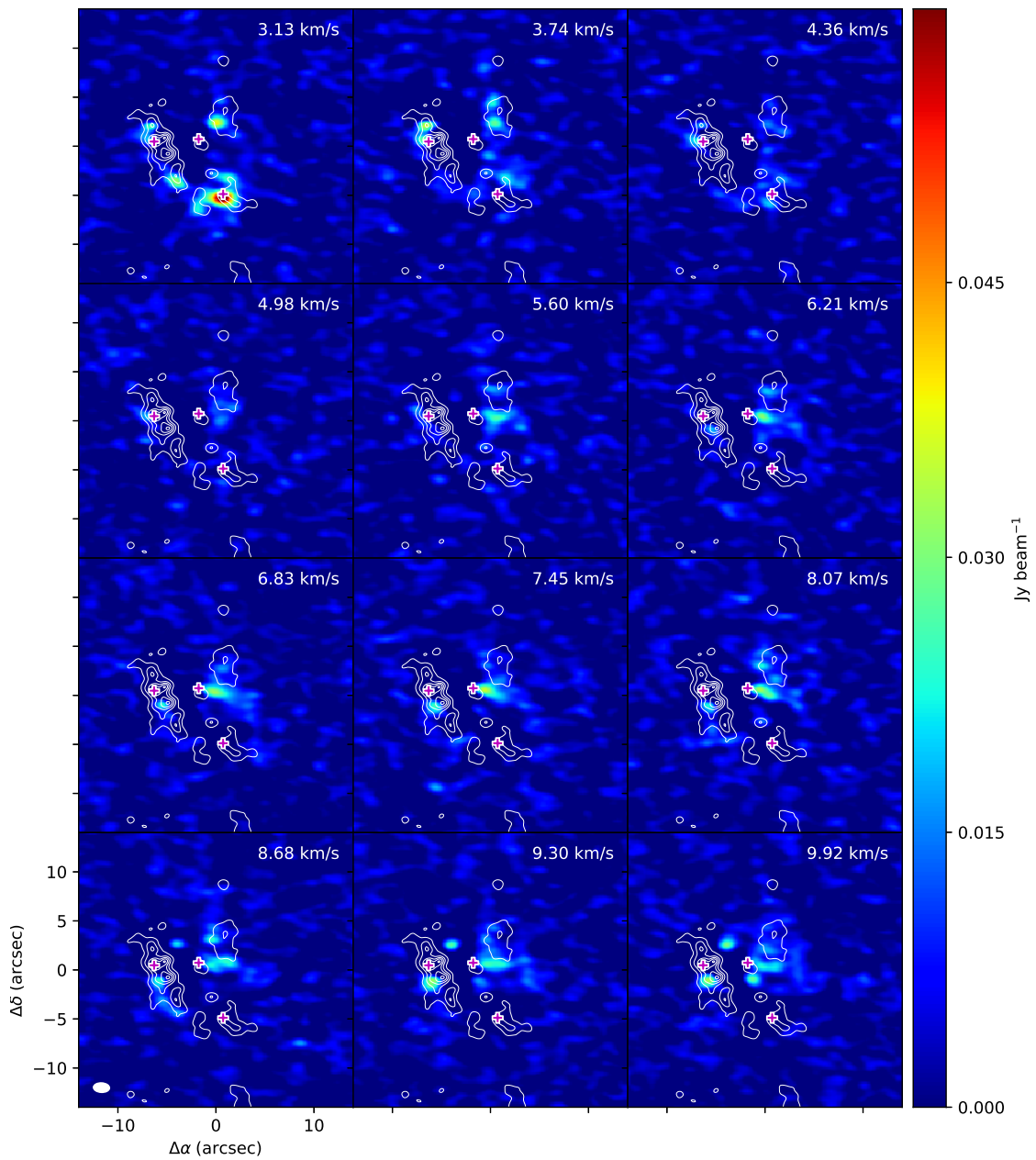


Figure A.19: 237.144GHz

# **Acknowledgments**

# References

- Hirota, T., Kim, M. K., Kurono, Y., & Honma, M. 2015, *The Astrophysical Journal*, 801, 82
- McMullin, J. P., Waters, B., Schiebel, D., Young, W., & Golap, K. 2007, in Astronomical Society of the Pacific Conference Series, Vol. 376, *Astronomical Data Analysis Software and Systems XVI*, ed. R. A. Shaw, F. Hill, & D. J. Bell, 127
- Pagani, L., Favre, C., Goldsmith, P. F., Bergin, E. A., Snell, R., & Melnick, G. 2017, *Astronomy & Astrophysics*, 604, A32
- Sanchez-Monge, A., Schilke, P., Ginsburg, A., Cesaroni, R., & Schmiedeke, A. 2017, STATCONT: Statistical continuum level determination method for line-rich sources, *Astrophysics Source Code Library*
- Turner, B. E. 1991, *The Astrophysical Journal Supplement*, 76, 617